A DYNAMICAL MODEL OF “QUASI-STATIONARY” STATES IN LARGE-SCALE ATMOSPHERIC MOTIONS(Dissertation_全文)

AUTHOR(S):

Mukougawa, Hitoshi

学位申請論文

向川　均

A Dynamical Model of "Quasi-Stationary" States in Large-Scale Atmospheric Motions

Hitoshi Mukougawa

Geophysical Institute, Kyoto University,
Kyoto 606, Japan.

November 1987

(submitted to J. Atmos. Sci.)

ABSTRACT

A theoretical study is made of the dynamics of 'quasi-stationary (QS)' states in large-scale irregular atmospheric motions by using a truncated, two-layer, quasi-geostrophic model in a β-channel. The model includes surface topography, external thermal forcing (*i.e.*, meridional differential heating) and dissipative processes. We define a QS state as a period when the magnitude of the time-derivative of spectral components $|\dot{x}(t)|$ is smaller than a prescribed threshold value.

For a wide range of parameter values of the thermal forcing, each QS state is found to occur when the trajectory $x(t)$ passes immediately next to a local minimum point (MP) of $|\dot{x}|$ in phase space. Moreover, we give the statistical significance to this relation between each QS state and an MP almost independent of the threshold value defining QS states. Therefore, the recurrence of the QS states is assured. The MP is either a stationary solution or a non-stationary minimum point bifurcating from a limit point of a stationary solution.

In irregular motions, some MPs are preferably selected to generate QS states independent of initial conditions. This selection does not depend on the local dynamical property of each MP, but is attributed to an inhomogeneous probability density distribution of the global trajectory in phase space.

The probability that each QS state persists over n days is well expressed as $\exp(-n/\tau)$, where τ is a characteristic time. This probability distribution is analytically deduced from a simple linearized system around an MP. We also obtain some examples of the linear growth of an unstable eigenmode of the nearest MP at the end of a QS state. These statistical and dynamical properties of the QS states support the relation between each QS state and an MP

1. Introduction

From the age of the synoptic meteorology, innumerable observations have elucidated that there are some quasi-stationary recurrent flow patterns in large-scale atmospheric motions of the extratropical troposphere. Among these patterns, the blocking phenomenon is one of the most attracting events for the meteorologists. Recently, some observational studies revealed the geographical distribution and the persistence of these patterns by adopting an objective definition for them (*e.g.*, Hartmann and Ghan, 1980; Dole, 1983).

Charney and DeVore(1979) gave a fresh insight into the dynamics of these patterns by introducing a concept of multiple stable equilibria of the large-scale states. By using the most severely truncated low-order barotropic model, they obtained two stable equilibrium states through the nonlinear interaction between the externally driven zonal flow and Rossby waves forced by surface topography and/or heat contrasts: One is connected with the "high-index" flow with a weak wave component and the other is related to the "low-index" (blocking) flow with a strong wave component. Since the transition between these two stable states does not spontaneously occur for a fixed external forcing, they hypothesized that these large-scale equilibrium states are unstable to smaller-scale perturbations which are not resolved in the low-order model, and hence these instabilities cause the transition between these large-scale states.

However, as Mukougawa(1987) revealed in a framework of the linear theory, the smaller-scale instabilities of topographically forced Rossby waves in a two-layer baroclinic model only act to diminish the basic waves and cannot cause the transition between the large-scale equilibrium states. Moreover, by using a nonlinear two-layer baroclinic model

with small-scale waves, Yoden(1983) (hereafter referred to as Y83) remarked that atmospheric motions are irregular in essence, where stationary solutions in the low-order model do not have any relevance at all. Therefore, the concept of multiple stable equilibria of the large-scale states has lost its theoretical premises.

On the other hand, Reinhold and Pierrehumbert(1982, 1985) (hereafter referred to as RP) first took notice of recurrent quasi-stationary features in the irregular motions by using a truncated two-layer model which includes highly baroclinically unstable wave components. They intuitively recognized two distinct time-mean states, "weather regimes"; the large-scale states aperiodically vacillate between these two weather regimes which are not located near any of the stationary equilibria of the large-scale state. Although the concept of the weather regime is very fascinating, the existence of these phenomena crucially depends on the number of retained components in the model as revealed by Cehelsky and Tung(1987). Furthermore, their definition of the weather regime is rather subjective. Therefore, the direct application of the concept of this weather regime to other dynamical systems and the real atmosphere is suspicious.

Recently, by using a truncated barotropic model on a sphere, Legras and Ghil(1985) (hereafter referred to as LG) examined recurrent features of persistent sequences ("planetary flow regimes") which are defined as periods when the variation of the trajectory in phase space within a sampling time interval is relatively small. From the resemblance of the flow pattern between each planetary flow regime and an unstable stationary solution, they concluded that each planetary flow regime occurs in the vicinity of an unstable stationary solution in phase space. The recurrent quasi-stationary features in their model were dynamically attributed to local properties of the unstable sta-

tionary solutions. However, there are some remaining problems in this idea:

(i) Is there any attractor generating quasi-stationary sequences except for stationary solutions? LG have noted the existence of such an attractor ("ghost" equilibrium) near a limit point of a stationary solution.

(ii) Are the quasi-stationary sequences dynamically related to these attractors in a baroclinic model? Although persistent sequences can be formally defined in any irregular motions, this relation is not accepted *a priori*. Therefore, it is necessary to make clear a condition under which this relation has the dynamical significance.

In this article, we carefully examine the dynamics of the quasi-stationary sequences in irregular motions by using a truncated two-layer, quasi-geostrophic, β-channel model with surface topography, external thermal forcing and dissipative processes in order to answer the above questions. We refer to the quasi-stationary sequences where the magnitude of the time-derivative of spectral components $|\dot{x}(t)|$ is smaller than a prescribed threshold value as "quasi-stationary (QS)" states. To explain recurrent features of these QS states, we hypothesize that each QS state occurs when the trajectory $x(t)$ passes immediately next to a local minimum point (MP) of $|\dot{x}|$ in phase space; the MP is either a stationary solution or a non-stationary minimum point. Although this hypothesis, which generalizes the connection between each QS state and a stationary solution found by LG, is trivial in motions of one dimension, the validity of this hypothesis is not necessarily recognized in motions in multi-dimensional phase space. Therefore, our main exertion is devoted to confirm the validity of this hypothesis in practice. Next, we develop statistics and dynamics of

the QS states to support this hypothesis. We also clarify the difference between the concept of QS states and that of the weather regimes proposed by RP

2. Model

a. *Model description*

A two-layer quasi-geostrophic model in a mid-latitude β-channel with surface topography is used (Fig.1). An external thermal forcing representing the differential solar heating between the equator and pole and dissipative processes are included in the model. The vorticity equations and thermodynamic equation are

$$\frac{\partial}{\partial t}\nabla^2\psi_l = -J(\psi_l,\nabla^2\psi_l+\beta y)+\frac{f_0}{\Delta p}(\omega_{l+1/2}-\omega_{l-1/2})-k\nabla^2\psi_l, \qquad l=1,2, \tag{2.1}$$

$$\frac{\partial}{\partial t}(\psi_1-\psi_2) = -\frac{1}{2}J(\psi_1+\psi_2,\psi_1-\psi_2)+\frac{S\Delta p}{f_0}\omega_{3/2}+\mu[\theta^*-(\psi_1-\psi_2)], \tag{2.2}$$

where the following notation is used:

t; time,

x; eastward coordinate,

y; northward coordinate,

∇^2; horizontal Laplacian operator $(=\partial^2/\partial x^2+\partial^2/\partial y^2)$,

$J(a,b)$; horizontal Jacobian operator $[=(\partial a/\partial x)(\partial b/\partial y)-(\partial a/\partial y)(\partial b/\partial x)]$,

$\psi_l(x,y,t)$; geostrophic stream function at the level l,

ω_l; vertical p-velocity at the level l,

f_0; Coriolis parameter at the center of the channel,

β; latitudinal variation of the Coriolis parameter,

Δp; pressure difference between the two level,

S; static stability parameter,

k; frictional coefficient,

μ; Newtonian heating coefficient,

$\theta^*(x,y)$; prescribed equilibrium potential temperature.

A cyclic channel of $2\pi L/\alpha$ in x-direction is considered:

$$\psi_l(x,y,t) = \psi_l(x+2\pi L/\alpha,y,t), \qquad l=1,2. \tag{2.3}$$

Two rigid walls of the channel are placed at $y=0$ and $y=\pi L$:

$$\frac{\partial\psi_l}{\partial x} = 0 \quad \text{and} \quad \int_0^{2\pi L/\alpha}\frac{\partial}{\partial t}(-\frac{\partial\psi_l}{\partial y})dx = 0, \qquad l=1,2, \tag{2.4}$$

at $y=0$ and $y=\pi L$.

As a lower boundary condition which represents the effect of surface topography, we adopt

$$\omega_{5/2} = -\rho_{5/2}gJ(\psi_2,h), \tag{2.5}$$

where $\rho_{5/2}$ is the density of the air at the level 5/2, g the gravitational acceleration and $h(x,y)$ the topographic height. The upper boundary condition is given by

$$\omega_{1/2} = 0. \tag{2.6}$$

Eliminating ω in (2.1) and (2.2) with (2.5) and (2.6), we obtain the following equations for $\varphi=(\psi_1+\psi_2)/2$ and $\theta=(\psi_1-\psi_2)/2$:

$$\frac{\partial}{\partial t}\nabla^2\varphi = -J(\varphi,\nabla^2\varphi)-J(\theta,\nabla^2\theta)-\beta\frac{\partial\varphi}{\partial x}-J(\varphi-\theta,h)-k\nabla^2\varphi, \tag{2.7}$$

$$\frac{\partial}{\partial t}(\nabla^2-\frac{1}{S})\theta = -J[\varphi,(\nabla^2-\frac{1}{S})\theta]-J(\theta,\nabla^2\varphi)-\beta\frac{\partial\theta}{\partial x}+J(\varphi-\theta,h)-k\nabla^2\theta-\frac{\mu}{S}(\theta^*-\theta), \tag{2.8}$$

where all variables and constants are non-dimensionalized: t is non-dimensionalized by $1/f_0$; x and y by L; φ and θ by L^2f_0; β by f_0/L; S by $2(Lf_0/\Delta p)^2$; and h by $(2\Delta p)/(\rho_{5/2}g)$, k and μ by f_0.

Equations (2.7) and (2.8) are identical to Eqs. (2.1)–(2.5) in Y83 except for the frictional processes; we introduce Rayleigh friction in the upper layer in stead of the internal friction between two layers. With this modification, we avoid the undesirable property in the system of Y83, where the 'Hadley' solution without wave components exists in spite of the existence of surface topography.

We expand φ, θ, θ^*, h in the following truncated orthonormal functions:

$$\begin{cases} F_{A_m} = \sqrt{2}\cos my, \\ F_{K_n^m} = 2\sin my\cos n\alpha x, \\ F_{L_n^m} = 2\sin my\sin n\alpha x, \qquad m=1,2,\cdots,M, \quad n=1,2,\cdots,N, \end{cases} \tag{2.9}$$

which satisfy the boundary conditions (2.3) and (2.4). Substituting the spectral expansion into (2.7) and (2.8), we finally obtain a set of $\nu=2M\times(2N+1)$ ordinary differential equations for the expansion coefficients $\varphi_C(t)$ and $\theta_C(t)$ (here, subscript C is one of A_m, K_n^m or L_n^m). These equations are symbolically written as

$$\dot{x}_i = \sum_j^{\nu}\sum_k^{\nu}(a_{ijk}x_jx_k+b_{ijk}x_jh_k)+\sum_j^{\nu}c_{ij}x_j+d_i, \qquad i=1,2,\cdots,\nu, \tag{2.10}$$

where x_i represents φ_C or θ_C, the first term on the right-hand side is the non-linear advection term, the second term represents the interaction with surface topography, the third term comes from β-effect and dissipation and the last term indicates the external thermal forcing.

b. *Parameter values and truncation level*

The lateral boundaries are placed at 20°N and 70°N. Therefore, L, f_0 and β with dimension are given by

$$\begin{cases} L = 1.77\times10^{6} \text{ m}, \\ f_0 = 1.03\times10^{-4} \text{ s}^{-1}, \\ \beta = 1.61\times10^{-11} \text{ m}^{-1}\text{s}^{-1} \end{cases} \tag{2.11}$$

The static stability parameter $S=2.83\times10^{-2}$ $\text{m}^2\text{s}^{-2}\text{mb}^{-2}$ and this value corresponds to the vertical difference of the potential temperature 30°K per 500 mb. We set $k=\mu$, of which value is given to have an e-folding time of 10.0 days.

The surface topography is assumed to have a sinusoidal shape with the zonal wavenumber α and the gravest meridional mode:

$$h = h_0 F_{kl} = 2h_0 \sin y \cos \alpha x. \tag{2.12}$$

In order to represent the land-sea distribution of the earth coarsely, the zonal wavenumber α is related to the planetary zonal wavenumber 3 in the latitude circle at 45°N by

$$\alpha = \frac{3L}{a \cos 45°}, \tag{2.13}$$

where a is the radius of the earth. The amplitude of surface topography ($2h_0$) is set 1 km. The above all parameter values are fixed in this study.

The prescribed equilibrium potential temperature θ^* is assumed to have the following zonally symmetric distribution:

$$\theta^* = \theta_A^* F_{A_1} = \sqrt{2}\theta_A^* \cos y, \tag{2.14}$$

which represents the temperature difference across the channel (ΔT). As the bifurcation parameter, we will change θ_A^* from 0.0 to 0.8 (the

corresponding ΔT is from 0°K to 52.3°K).

The truncation level adopted in this study is M=2 and N=3 in (2.9). Therefore, we have a forced-dissipative system with 28 degrees of freedom. This truncation is identical to Case 3 in Y83 and organizes the smallest system retaining the following important nonlinear interactions (see Y83; Cehelsky and Tung, 1987): (i) all components are linked with the triad interactions; (ii) all wave components interact with surface topography of (1, α) component. Hereafter, the first integer in each parenthesis refers to the meridional mode and the second one the zonal wavenumber.

c. *Dynamical characteristics in the truncated system*

We remark two dynamical characteristics in this truncated system. One is the symmetry group of the spectral components. As Yoden(1985) indicated, the orthonormal functions in this channel geometry are divided into two groups: S-mode and T-mode components according to whether they are invariable under a transformation T:

$$Z(x,y) \rightarrow -Z(x+\pi/\alpha,\pi-y). \tag{2.15}$$

S-mode components consist of

$$\begin{cases} F_{A_m}; \ m=\text{odd and} \\ F_{K_{mn}},\ F_{L_{mn}}; \ m+n=\text{even}, \end{cases} \tag{2.16}$$

which satisfy $F_{S_i}(x,y)=T[F_{S_i}(x,y)]$, and T-mode components consist of

$$\begin{cases} F_{A_m}; & m=\text{even and} \\ F_{K_n},\ F_{L_n}; & m+n=\text{odd}, \end{cases} \tag{2.17}$$

which satisfy $F_{T_i}(x,y)=-T[F_{T_i}(x,y)]$. Here, the subscript S_i and T_i denote each group of the orthonormal functions.

Now, Eq. (2.10) is divided into the following two groups [see (2.15) and (2.16) in Yoden, 1985]:

$$\dot{x}_{S_i} = \sum_j \sum_k (a_{S_iS_jS_k} x_{S_j} x_{S_k} + a_{S_iT_jT_k} x_{T_j} x_{T_k} + b_{S_iS_jS_k} x_{S_j} h_{S_k}) + \sum_j c_{S_iS_j} x_{S_j} + d_{S_i}, \tag{2.18}$$

$$\dot{x}_{T_i} = \sum_j \sum_k (a_{T_iS_jT_k} x_{S_j} x_{T_k} + a_{T_iT_jS_k} x_{T_j} x_{S_k} + b_{T_iT_jS_k} x_{T_j} h_{S_k}) + \sum_j c_{T_iT_j} x_{T_j}. \tag{2.19}$$

Here, we have taken account of the horizontal shape of surface topography and thermal forcing adopted in this study ($h_{T_i}=0$ and $d_{T_i}=0$). Then, the following characteristics which generalize the results in Yoden(1985) are found in (2.18) and (2.19):

(i) If $\{\dot{x}_{S_i},\ \dot{x}_{T_i}\}$ is given by $\{\alpha_{S_i},\ \alpha_{T_i}\}$ when $\{x_{S_i},\ x_{T_i}\}=\{\beta_{S_i},\ \beta_{T_i}\}$, then $\{\dot{x}_{S_i},\ \dot{x}_{T_i}\}=\{\alpha_{S_i},\ -\alpha_{T_i}\}$ when $\{x_{S_i},\ x_{T_i}\}=\{\beta_{S_i},\ -\beta_{T_i}\}$. Here, β_i are arbitrary real constants.

(ii) When $\{x_{S_i},\ x_{T_i}\}=\{\beta_{S_i},\ 0\}$, $\dot{x}_{T_i}=0$. Thus, S-mode components organize a sub-system of Eq. (2.10).

Furthermore, in the linearized equations of (2.10):

$$\dot{x}_i' = \sum_j^{\nu} \sum_k^{\nu} [a_{ijk}(x_j' \bar{x}_k + \bar{x}_j x_k') + b_{ijk} x_j' h_k] + \sum_j c_{ij} x_j', \qquad i=1,2,\cdots,\nu, \tag{2.20}$$

for the deviation $x_i'(t)$ from a basic state $\overline{x_i(t)}$, the following property is found:

(iii) If an eigenvector corresponding to an eigenvalue σ is given by $\{\zeta_{S_i},\ \zeta_{T_i}\}$ for a basic state $\{\bar{x}_{S_i},\ \bar{x}_{T_i}\}$, an eigenvector $\{\zeta_{S_i},\ -\zeta_{T_i}\}$ corresponds to the eigenvalue σ for a basic state $\{\bar{x}_{S_i},\ -\bar{x}_{T_i}\}$.

From the above properties, it is found that two states which are con-

verted into each other by the transformation T of (2.15) are equivalent in dynamical properties.

The other characteristic in this truncated system is that the most severely truncated system M=N=1 in (2.9) forms a sub-system of the full system M=2, N=3 (see Y83). However, this property is not retained in less truncated systems (see Cehelsky and Tung, 1987).

3. Local minimum point of $|\dot{x}|$ in phase space

a. General description of MP

We develop general description about a local minimum point (MP) of $|\dot{x}|=[\sum_{i=1}^{\nu}(\dot{x}_i)^2]^{1/2}$ in ν-dimensional phase space of (2.10). First of all, an MP must be a solution of the following equation:

$$\nabla X = 2J^T\dot{x} = 0, \tag{3.1}$$

where

$$X = \sum_{i=1}^{\nu}(\dot{x}_i)^2,$$

and

$$J = \begin{pmatrix} \frac{\partial\dot{x}_1}{\partial x_1} & \frac{\partial\dot{x}_1}{\partial x_2} & \cdot & \frac{\partial\dot{x}_1}{\partial x_\nu} \\ \frac{\partial\dot{x}_2}{\partial x_1} & \frac{\partial\dot{x}_2}{\partial x_2} & \cdot & \frac{\partial\dot{x}_2}{\partial x_\nu} \\ \cdot & \cdot & \cdot & \cdot \\ \frac{\partial\dot{x}_\nu}{\partial x_1} & \frac{\partial\dot{x}_\nu}{\partial x_2} & \cdot & \frac{\partial\dot{x}_\nu}{\partial x_\nu} \end{pmatrix}. \tag{3.2}$$

Moreover, a solution of (3.1) is classified as follows:

$$\begin{cases} \sigma_i>0 \quad i=1,\cdots,\nu\text{: local minimum point (MP),} \\ \sigma_i<0 \quad i=1,\cdots,\nu\text{: local maximum point,} \\ \text{otherwise:} \quad \text{saddle point,} \end{cases} \tag{3.3}$$

where σ_i is an eigenvalue of H:

$$H = \begin{pmatrix} \frac{\partial^2 X}{\partial x_1^2} & \frac{\partial^2 X}{\partial x_1 \partial x_2} & \cdot & \frac{\partial^2 X}{\partial x_1 \partial x_\nu} \\ \frac{\partial^2 X}{\partial x_2 \partial x_1} & \frac{\partial^2 X}{\partial x_2^2} & \cdot & \frac{\partial^2 X}{\partial x_2 \partial x_\nu} \\ \cdot & \cdot & \cdot & \cdot \\ \frac{\partial^2 X}{\partial x_\nu \partial x_1} & \frac{\partial^2 X}{\partial x_\nu \partial x_2} & \cdot & \frac{\partial^2 X}{\partial x_\nu^2} \end{pmatrix} \tag{3.4}$$

which is the Hessian matrix of X. From (3.1), we find that the MP is either a stationary solution which satisfies $\dot{x}=0$ or a non-stationary minimum point (MIN) at which $\dot{x}\neq 0$ but at least one eigenvalue of J^T of (3.2) is zero.

Without loss of generality, the bifurcation theory of stationary solutions can be directly applied to bifurcations of MINs if the equation $\dot{x}=0$ is replaced by the equation $\nabla X=0$ and the Jacobian J of $\dot{x}$ by the Hessian H of X in that theory. Some simple critical points of an MIN are shown in Fig.2; at these points one eigenvalue of H becomes zero. When the bifurcation parameter λ passes the "limit point" (Fig.2-a), a pair of an MIN (solid line) and a saddle point (broken line) suddenly appears. At the "bifurcation point", a branch of an MIN changes into a branch of a saddle point and a new pair of MINs (saddle points) appears to the super-critical (sub-critical) side of that point in parameter space as in Fig.2-(b) (Fig.2-c). It is also found that the "Hopf-bifurcation point" of an MIN does not exist; all eigenvalues of H are necessarily real numbers because H is a symmetric matrix.

Next, we investigate an important relation between the appearance of an MIN and the simple critical points (*e.g.*, limit point and bifurcation point) of stationary solutions. Since J has a zero eigenvalue at these points, we can anticipate the generation of an MIN from these points by taking account of (3.1). Some illustrative examples are shown

in Fig.3. Figure 3-(a) shows the appearance of an MIN (thin solid line) to the sub-critical side of the limit point of a pair of stationary solution branches (thick solid line); This configuration is equivalent to the super-critical "bifurcation point" of an MIN in Fig.2-(b). On the other hand, we find that the bifurcation point of stationary solutions does not generate any MIN as in Fig.3-(b). These relations between the appearance of an MIN and the simple critical points of stationary solutions can be generalized in any dynamical systems (H. Fujii, personal communication, 1987).

b. *MP in our truncated system*

Two numerical methods are used to obtain MPs in our truncated nonlinear system (2.10). First, we use the revised Marquardt method (see Yoden, 1985; Iwashima and Yamamoto, 1986), which minimizes X in (3.1) from a specified initial guess. Here, several hundreds of initial guesses are given for several prescribed values of θ_A^*. We discriminate between a stationary solution and an MIN by the value of $|\dot{x}|$ at the obtained MP. Figure 4 shows the distribution of $|\dot{x}|$ on the segment containing a stationary solution (S2) and an MIN (M7) in phase space (θ_A^*=0.054); The value of $|\dot{x}|$ has a small finite value at the MIN, but becomes as small as the round off errors of the computer at the stationary solution.

Second, we trace a solution branch of $\dot{x}$=0 (∇X=0) from a stationary solution (MIN) obtained by the above method with changing the value of the parameter θ_A^* by using a continuation method of Kubíček and Marek(1983) (see also Iwashima and Yamamoto, 1986). Furthermore, we systematically utilize the dynamical characteristics of our system discussed in Section 2.c, so we think that all MPs have been obtained for parameter values which are relevant in the following investigations.

1) STATIONARY SOLUTION

Thick lines in Fig.5 denote branches of stationary solutions. The abscissa is the bifurcation parameter θ_A^* and the ordinate indicates the gravest barotropic zonal component φ_{A_1}. We refer to some relevant branches as S1, S2, ···, S5 which are written on the corresponding branches. Linear stability of the stationary solution is investigated by solving an eigenvalue problem of the linearized equations of (2.20), and is indicated on the branches by a symbol s (stable) or u (unstable). It is also noted here that two branches of stationary solutions such as S2 and S3 which are converted into each other by the transformation T of (2.15) are degenerated into one line in this figure. These two solutions have all the same stability characteristics as discussed in Section 2.c.

The stream function of all stationary solutions at $\theta_A^*=0.054$ is presented in Fig.6. The horizontal pattern of stationary solutions on the same branch is qualitatively similar in the parameter range in Fig.5 ($0.03 \leqq \theta_A^* \leqq 0.08$). The stationary solution S1, which is a solution of the sub-system $M=1$ and $N=1$ in (2.9), arises from the trivial solution ($x=0$) at $\theta_A^*=0$. This solution is stable for $0 \leqq \theta_A^* \leqq 0.0317$. At $\theta_A^*=0.03173$ (denoted by B in Fig.5), S2 and S3 appear from S1 by a bifurcation with symmetry breaking (see Fig.6). These two solutions are stable only for a narrow parameter range of $0.0317 \leqq \theta_A^* \leqq 0.0349$. For $\theta_A^* \geqq 0.035$, all stationary solutions are unstable to an infinitesimal perturbation, therefore, multiple stable equilibria do not exist for a wide range of parameters in this model.

2) MIN

Table 1 shows the list of all MPs at $\theta_A^*=0.054$. We refer to respective MINs existing at $\theta_A^*=0.054$ as M1, M2, ···, M14, MS1, MS2, of which

symbols are put on the corresponding branches in Fig.5; Note that M13, M14 and MS2 protrude from Fig.5 (see the second column of Table 1). Two branches of MINs such as M1 and M2 which have the same dynamical properties are merged into one line in Fig.5 as the stationary solutions S2 and S3. In Table 1, these couples of MINs are also listed in same rows.

Some peculiar properties are found in MS1 and MS2: (i) MS1 and MS2 are referred to respective groups of innumerable points consisting only of S-mode components; (ii) Among these points in each group, all components have same values except for components (2, 2α) and (1, 3α); (iii) The value of $|\dot{x}|$ has a same value at these points; (iv) One eigenvalue of H is zero at these points. From these properties, we conclude that MS1 and MS2 form valleys of $|\dot{x}|$ in phase space, respectively. Moreover, since MS1 and MS2 appear at $\theta_A^*\neq 0.0317$ where the bifurcation of S1 with symmetry breaking occurs (Fig.5), the existence of MS1 and MS2 may be ascribed to the symmetry of the channel geometry.

Figure 7 shows the upper-layer stream function of all MINs at $\theta_A^*=0.054$. The horizontal pattern of MINs on the same branch is qualitatively similar as that of stationary solutions. Only one point is presented in this figure for MS1 and MS2; Spatial patterns of other points belonging to MS1 and MS2 are similar to the examples in Fig.7 except for a phase shift in x-direction, so MS1 and MS2 can be easily separated from other MPs by visual inspection.

It is found from Fig.5 that some MINs actually bifurcate from limit points of the stationary solution as in Fig.3-(a); *e.g.*, M3 and M4 bifurcate from 'L of S4 and S5. Other MINs which are not connected with any limit point of the stationary solution in this bifurcation parameter may be generated from limit points in other external parameter values, such as k the frictional coefficient. The relation between

the MIN and the corresponding limit point of the stationary solution is also intuitively understood from the comparison between Fig.7 and Fig.8 which shows the upper-layer stream function of S4 at its limit point (denoted by L in Fig.5). An excellent resemblance of patterns is found between M3 in Fig.7 and S4 in Fig.8. From the above connections between the MIN and the limit point of the stationary solution, we can conclude that the "ghost" equilibrium noted by LG, which was recognized as persistent sequences existing near a limit point of the stationary solution in numerical time-integrations, corresponds to the MIN.

Finally, it is also found from Fig.5 that some branches of MINs disappear at some values of θ_A^*, where the MIN changes into a saddle point through the "limit point" revealed in Fig.2-(a). Moreover, any MIN does not appear from the bifurcation point of S1 in consistence with the configuration in Fig.3-(b).

4. Routes to chaos

We have performed a series of time-integration of (2.10) from the stationary solution S1 with several infinitesimal perturbations for some specified θ_A^* by using the Adams-Bashforth-Moulton formulas of a variable order with an automatic step-size control (see Kubíček and Marek, 1983). We present the asymptotic behavior appearing in each integration.

The result is summarized in Fig.9. Figure 10 shows several temporal variations of φ_{A_0}, whose power spectral density by using the FFT method is shown in Fig.11. For $\theta_A^* \leq 0.0317$, only the stable solution S1 appears. For $0.0318 \leq \theta_A^* \leq 0.0349$, the solution converges into the stable equilibrium S2 or S3 according to the initial condition. Multiple stable periodic solutions appearing from the Hopf-bifurcation of S2 and S3 at $\theta_A^*=0.03491$ (denoted by H in Fig.5) exist for $0.035 \leq \theta_A^* \leq 0.038$. These periodic solutions bifurcate into aperiodic solutions through intermittent behavior for $0.040 \leq \theta_A^* \leq 0.060$. Figure 10-(a) represents the intermittent behavior at $\theta_A^*=0.040$, where chaotic noise disturbs the almost periodic sequences, and spectral peaks are obscure (Fig.11-a). For $\theta_A^*=0.058$ and 0.060, there is a stable periodic solution (Fig.10-b, Fig.11-b) which is coexisting with an aperiodic solution (Fig.10-c, Fig.11-c). For $\theta_A^*=0.062$ and 0.064, we did not obtain any aperiodic solutions, but a quasi-periodic solution appears (Fig.10-d, Fig.11-d); In the quasi-periodic motion at $\theta_A^*=0.062$, the frequency of all spectral peaks is represented by a linear combination of three irrational frequencies: f_1, f_2 and f_3 denoted in Fig.11-(d). This motion develops into fully aperiodic motions for $\theta_A^* \geq 0.066$ (Fig.10-e, Fig.11-e). Compared with preexisting aperiodic motions for $0.040 \leq \theta_A^* \leq 0.060$, these motions have much energy in high-frequency domain because of the increase of

the baroclinicity.

We did not detect any 'weather regime' phenomenon of RP in these aperiodic motions.

5. "Quasi-stationary" state

a. *Definition and hypothesis*

In order to elucidate recurrent quasi-stationary features in aperiodic motions, we examine sequences of relatively slow variations where the magnitude of the time-derivative of spectral components is smaller than a prescribed threshold value, *i.e.*,

$$|\dot{x}| \leq C_0, \tag{5.1}$$

where C_0 is a positive definite value. We refer to this state as "quasi-stationary (QS)" state. This definition of QS states is equivalent to that of persistent regimes in LG when a sampling time interval τ in Eq. (11) of LG approaches zero. Our definition has an advantage that it is independent of the time-scale of motions.

In this study, we hypothesize that each QS states is dynamically connected with a preferred point of MPs in phase space. We will verify our hypothesis by indicating that each QS state occurs when the trajectory $x(t)$ passes immediately next to an MP.

b. *Verification of our hypothesis*

As an example, we use data of 5000 days with asymptotic behavior which are sampled every day at $\theta_A^{\dagger}$=0.054. Figure 12 shows the time variation of $|\dot{x}|$. The local minima of $|\dot{x}|$ are quite flat compared to the local maxima; this feature was also captured in Fig.10 of LG. At the beginning, we tentatively define QS states by adopting $[|\dot{x}|]-\sigma(|\dot{x}|)$ as C_0 in (5.1). Hereafter, $[\alpha]$ and $\sigma(\alpha)$ represent the time-mean and standard deviation of α for the interval of data. The horizontal solid line in Fig.12 denotes $[|\dot{x}|]$ and the broken line is $[|\dot{x}|]-\sigma(|\dot{x}|)$. The period

of each QS state is indicated by a vertical line whose width is its duration time. The value of $|\dot{x}|$ in this aperiodic motion is at least twice as large as that of $|\dot{x}|$ at MPs (see the third column of Table 1). Thus, the verification of our hypothesis on the relation between each QS state and an MP needs a careful examination.

We calculate *distance* between $x(t)$ and all MPs in phase space. Here, *distance* between two points, x and y, is defined as a square root of the summation of $(x_i-y_i)^2$ over all components except for components (2, 2α) and (1, 3α). With this definition of *distance*, MS1 and MS2 consisting of innumerable points are respectively recognized as one point in phase space. Figure 13 shows *distance* from the nearest MP (solid line) and *distance* from the second-nearest MP (broken line) at every day. It is clear that *distance* from the nearest MP during each QS period is much smaller than that in other ("non-QS") periods, but *distance* from the second-nearest MP during each QS period is comparable to that in non-QS periods; This intuitively suggests the occurrence of each QS state in the vicinity of an MP Furthermore, so as to visualize the relation between a QS state and an MP, we show stream function fields during a QS state which occurs near M8 for day 1210-1217 in Fig.14; The excellent resemblance to M8 in Fig.7 is obtained.

Next, we attempt to verify our hypothesis on the relation between each QS state and an MP statistically. This relation should be statistically verified if the following conditions are satisfied:

$$\text{(i)}\ [|DX_1|_{\text{at } t=t_n}]_{QS} \leq [|DX_1|]_{\text{non-QS}} - \sigma([|DX_1|)_{\text{non-QS}},$$
$$\text{(ii)}\ [|DX_2|_{\text{at } t=t_n}]_{QS} \geq [|DX_2|]_{\text{non-QS}} - \sigma(|DX_2|)_{\text{non-QS}}, \qquad (5.2)$$

where $|DX_1|$ ($|DX_2|$) is *distance* between $x(t)$ and the nearest

(second-nearest) MP; t_* denotes the time when $|DX_1|$ has the smallest value during a QS period; $[a]_{QS}=(\sum_{i=1}^{NQ}a)/NQ$ where NQ is a number of QS states in the data; $[a]_{non\text{-}QS}$ indicates the time-mean of a during non-QS periods; $\sigma(a)_{non\text{-}QS}$ is the standard deviation of a during non-QS periods. We adopt this condition to aim at representing the following circumstance: during a QS state $x(t)$ exists in such vicinity of an MP that *distance* from the MP is significantly small, but $x(t)$ does not exist in the statistically significant vicinity of other MPs.

Figure 15 shows that the condition (5.2) is well satisfied for QS states at $\theta_A^*=0.054$ regardless of the value C_0 in (5.1). The abscissa of this figure is a prescribed value C which gives C_0 for the definition of QS states with $C_0=[|\dot{x}|]+C\sigma(|\dot{x}|)$. In Fig.15-(a), the shaded region indicates the range of $[|DX_1|]_{non\text{-}QS}\pm\sigma(|DX_1|)_{non\text{-}QS}$ and the thick solid line is $[|DX_1|_{\ at\ t=t_*}]_{QS}$. This solid line is well separated from the shaded region for any C, so the condition (i) is well satisfied. On the other hand, the solid line exists in the shaded region except for $-1.5\leq C\leq -1.4$ in Fig.15-(b), which shows the corresponding quantities for $|DX_2|$. Thus, the condition (ii) is also satisfied for a wide range of C. The smoothness of the time variation of $|\dot{x}|$ near local minima of $|\dot{x}|$ in Fig.12 produces such an independent property of C_0. Hereafter, we proceed our discussions of QS states by setting $C=-1$.

c. Parameter dependence

We examine in what range of parameter θ_A^* the relation between each QS state and an MP exists (Fig.16). For each θ_A^*, the data used in calculating several quantities in (5.2) consist of a 5000-day record with asymptotic behavior in a numerical time-integration from the vicinity of the steady solution S1. For $\theta_A^*=0.058$ and 0.060, a record of an aperiodic solution is adopted in stead of a periodic solution. The

condition (5.2) is satisfied in aperiodic motions for a wide range of parameter values of $0.042 \leqq \theta_A^* \leqq 0.060$ and $0.066 \leqq \theta_A^* \leqq 0.072$. For $\theta_A^* = 0.040$, the condition (ii) is violated (Fig.16-b) because two stationary solutions exist immediately next to each other in phase space by the fold of the branches S2 and S3 (Fig.5). For $0.062 \leqq \theta_A^* \leqq 0.064$, where $x(t)$ quasi-periodically varies in a narrow phase space (this is suggested by a small value of $\sigma(|DX_1|)_{non\text{-}QS}$ and $\sigma(|DX_2|)_{non\text{-}QS}$), the condition (i) is not satisfied. For $\theta_A^* \geqq 0.074$, the condition (ii) is not satisfied. The trajectory of $x(t)$ is repelled by vigorous baroclinic eddies far from regions where all MPs exist, which is implied by a large value of $[|DX_1|]_{non\text{-}QS}$ and $[|DX_2|]_{non\text{-}QS}$. Therefore, it is not statistically significant to find the nearest MP during each QS period for these parameter ranges.

6. Statistical properties of QS states

On the basis of our hypothesis which has been statistically verified in the previous section for a wide range of the parameter values, we classify each QS state according to the nearest MP in phase space from the time-mean state during each QS period. We have also succeeded in dynamically explaining the recurrent features of QS states. In the following two sub-sections, we examine QS states at θ_A^*=0.054 in detail to discuss their statistics.

a. *Selection of MPs in generating QS states*

We investigate whether each MP has an equal probability to generate QS states in irregular motions. To reduce the dependence on the initial condition, we have proceeded numerical time-integrations from the vicinity of each MP at θ_A^*=0.054. Table 2 shows numbers of QS states occurring in the vicinity of each MP The data consist of a 2000-day record with asymptotic behavior for each initial condition: (a), (b), ···, (n) of which value is given in the legend of Table 2. QS states are defined from each 2000-day statistics of $|\dot{x}|$. Here, we put together numbers of QS states occurring near each couple of MPs having the same dynamical properties in a same column.

It is clear from this table that there is distinguished selection of MPs in generating QS states independent of initial conditions: S2, S3, M3, M4, M7, M8 and MS1 have several times lager probability to generate QS states than other MPs. We examine some causes of this selection from the following two viewpoints:

1) LOCAL DYNAMICAL PROPERTY OF MP

Since the magnitude of $|\dot{x}|$ at the MP is much smaller than that

in aperiodic motions (see the third column of Table 1), a QS state will be inevitably generated if $x(t)$ passes in the neighborhood of any MP. Therefore, the local dynamical property to attract $x(t)$ into such vicinity of an MP affects this selection of MPs. The number and magnitude of unstable/stable eigenvalues of the MP represent this property; The linearized motion around an MIN well describes the motion in the vicinity of MIN as that around a stationary solution, if $|\dot{x}|$ at the MIN is small enough to be neglected as in our model (see Appendix A).

In the fourth column of Table 1, all unstable eigenvalues of each MP are listed; Here, eigenvalues of MS1 and MS2 are not listed because stability properties are not the same among points belonging to MS1 and MS2. The dimension of the repelling sub-space from each MP, *i.e.*, the number of unstable eigenvalues, is much smaller than the dimension of our system. Thus, we conjecture that the local dynamical property of the MP cannot produce such definite selection of MPs. As calculated in Appendix B in practice, all MPs can attract almost all trajectories into the vicinity of the MP in the linearized system around the MP. Therefore, the selection of MPs is not attributed to the local dynamical property of the MP.

2) GLOBAL PROPERTIES OF TRAJECTORIES

Another factor to cause the selection of MPs is an inhomogeneous distribution of probability density of the trajectory in phase space. Such inhomogeneity is revealed in the second column of Table 3, in which each day in all the data sets of Table 2 is classified according to the nearest MP A large number of QS states for an MP tends to correspond to a large number of the proximity for that MP with a few exceptions, which implies that the selection of MPs is attributed to this factor

However, the ratios of each number in the third column against that in the second of Table 3 are not constant among MPs. Only differences in the geometrical feature of the surface $|\dot{x}|=C_0$ around each MP, inside of which QS states are defined, contribute to the difference of these ratios, because almost all trajectories on that surface are attracted into the vicinity of the MP as mentioned above. The fourth and the fifth columns in Table 3 indicate the maximum and minimum values of *distance* from the MP during QS states occurring in the vicinity of the MP, while the sixth and seventh columns are those during non-QS states. Both QS and non-QS states occur in a wide range of *distance* from each MP. This fact suggests a complicated feature of that surface in phase space. This complexity is also convinced from Fig.13; there are some periods when the trajectory passes in the neighborhood of an MP but $|\dot{x}|$ is not small enough for the state to be defined as a QS state.

b. *Duration of QS states*

The solid lines in Fig.17 show the number of QS states persisting over n days in the vicinity of some MPs. Here the same data sets in the previous sub-section are used, and QS states occurring in the vicinity of the two dynamically equivalent MPs are combined. These lines are well represented by lines of $A\exp(-t/\tau)$, where A and τ are constants. The broken lines are computed using a least squares program where we ignore data points of which event number is below 10. The characteristic time τ of each group of QS states has a value of 5 ~ 6 days except for MS1; this peculiar persistent characteristic of QS states near MS1 may result from the fact that MS1 consists of innumerable points having different dynamical properties (see Section 6.a). Therefore, the probability of the termination of a QS state does not

depend on its duration. Compared with the characteristic time of persistent regimes in LG, that of QS states in our model is much small, because of the presence of high-frequency baroclinic eddies.

This persistence distribution of QS states is also analytically deduced from a simple linearized system around an MP (see Appendix C). Thus, these statistics on the duration of QS states support our hypothesis on the relation between each QS state and the corresponding MP.

7. Temporal evolution of QS states

We show additional verification of our hypothesis on the relation between each QS state and an MP by exemplifying the following dynamical consequence (see LG; Ghil and Childress, 1987): When the solution vector $x(t)$ approaches an MP in phase space at the beginning of a QS state, its trajectory must exist in a sub-space spanned with stable eigenvectors of the MP. On the other hand, $x(t)$ must leave the MP on a sub-space containing unstable eigenvectors of the MP at the end of the QS state.

We expand the deviation vector $x'(t)$ from the nearest MP (x_{MP}) during a QS state into eigenvectors ζ_i ($i=1,\cdots,\nu$) of x_{MP} as follows:

$$\begin{aligned} x'(t) &= x(t)-x_{MP} \\ &= \sum_{i=1}^{\nu} c_i(t)\zeta_i, \end{aligned} \tag{7.1}$$

where ζ_i satisfies the eigenvalue problem of (2.20), which is written as $\sigma_i\zeta_i=L\zeta_i$ in the vector form, and the complex expansion coefficient $c_i(t)$ is derived from

$$c_i(t) = \frac{(x'(t)\cdot\xi_i)}{(\zeta_i\cdot\xi_i)}, \tag{7.2}$$

by using the orthogonality $(\zeta_i\cdot\xi_j)=0$ for $i\neq j$. Here, $(\cdot)$ indicates the inner-product and ξ_i is the adjoint eigenvector of ζ_i; ξ_i satisfies the adjoint eigenvalue problem of $\sigma_i\xi_i=L^T\xi_i$. Note that the eigenvector ζ_i does not make an orthonormal basis because the matrix L of this eigenvalue problem is not a normal matrix.

As an instance of the growth of an unstable eigenmode at the

end of a QS state, we examine a QS state occurring in the vicinity of S2 at θ_A^*=0.054. Figure 18 shows the time variation of $|\dot{x}|$ in 40 days including this QS period. The time variation of complex expansion coefficient (7.2) of the most unstable eigenmode of S2 (see Table 1) from day 4222 (denoted by S) to day 4236 (denoted by E) is plotted in the solid line in polar diagram of Fig.19. The broken line in Fig.19 denotes the time evolution of the complex amplitude of this unstable eigenmode after day 4222 when its linear growth is assumed. The excellent correspondence between these two lines confirms the detection of the linear growth of this eigenmode at the end of this QS state.

Moreover, the predominance of this eigenmode in the deviation field at the end of this QS state is found in Fig.20: Fig.20-(a) shows the sequence of the upper-layer stream function of the deviation field, while Fig.20-(b) shows that of this unstable eigenmode of which complex amplitude is given by (7.2). The deviation field is well represented only by this unstable eigenmode. In particular, the predominance of this unstable eigenmode is distinctively detected at the transient state at day 4236 when $|\dot{x}|$ has a local maximum value. This unstable eigenmode has the characteristics of baroclinic disturbances in which the component of zonal wavenumber 6 dominates.

We did not observe such prominent growth of an unstable eigenmode at the end of all QS states in our model. For lack of the orthogonality in the eigenvector ζ_i, the growth of one eigenmode inevitably has the projection on other eigenmodes. Therefore, such a distinctive detection becomes difficult. The access on a stable eigenmode into an MP at the commencement of a QS state is hardly detected, because the sub-space spanned with these stable eigenvectors occupies almost all phase space as discussed in Section 6.α (see the fourth column of Table 1).

8. Discussion

We proposed a concept of "quasi-stationary" states in aperiodic motions. Now, we clarify the difference between the concept of QS state and that of the weather regime proposed by RP. The difference is obvious in Fig.21, which shows the time variation of the amplitude (Fig.21-a) and phase (Fig.21-b) of the most gravest barotropic wave component in the demonstration case in RP. The time variation of $|\dot{x}|$ in this case is also shown in Fig.21-(c), where the weather regime is defined by visual inspection of the phase variation as in RP [designated by R (the ridge regime) and T (the trough regime)]. Each period of QS states is also indicated in this figure. The periods of weather regimes do not correspond to those of QS states, because the amplitude of that wave varies in time during each weather regime.

Recently, Mo and Ghil(1987a, b) extended the work of LG in two directions to apply the concept of the persistent regime to the real atmosphere. Here, we concentrate our discussions on their analysis of the model data which are identical to those of LG. Mo and Ghil(1987a) defined quasi-stationary patterns by using the horizontal pattern correlation in stead of phase-space velocity of trajectories, and obtained quasi-stationary patterns which are not detected in LG. This discrepancy arises because the pattern correlation cannot recognize amplitude variations of the pattern. However, if we emphasize dynamical aspects of quasi-stationary states, it is much easier to understand our (and LG's) definition of QS states than that of Mo and Ghil(1987a), because our definition is directly based on the governing equation of the system. On the other hand, Mo and Ghil(1987b) have developed a cluster analysis to obtain frequently recurrent patterns which include not only QS states but also transient states. However, since QS states do not

necessarily correspond to frequently recurrent patterns (see Table 3), this skillful method is apt to miss to detect non-frequent QS states.

It is worthwhile to comment on transient states where $|\dot{x}|$ has a large value. These transient states are easily classified into some recurrent patterns by visual inspection as noted in LG. To reveal the recurrence of these transient patterns dynamically, we tried to obtain local maximum points and saddle points of $|\dot{x}|$ in phase space. However, any local maximum point was not obtained nor the obtained saddle points did not have any resemblance to these transient states. Therefore, we did not have any dynamical explanation to these transient states, but we conjecture that the growth of an unstable eigenmode of the nearest MP of the previous QS state is a clue to understand the transient state. In some transient states, the deviation field from that MP is well represented by an unstable eigenmode of the MP as in Fig.20. Thus, these transient states may correspond to *exits* of an attractor basin of that MP. Moreover, the smallness of the number of unstable eigenmodes, *i.e.*, the *exits*, may explain the recurrent feature of the transient states. We expect that investigations of the transient state will inevitably develop our understanding of the transition mechanism between QS states.

In this paper, recurrent quasi-stationary features in the real atmosphere are not discussed in connection with the QS states in our simple mechanistic model, because our main purpose is to obtain the conceptual understanding of QS states in irregular motions. However, if we aim at applying our concept of QS states to the real atmosphere, we must examine the relation between each QS state and an MP in less truncated models and GCMs to explain the recurrence of QS patterns in the real atmosphere dynamically. In this expansion of our model, we conjecture that small-scale components retained in these models do

not invalidate this relation from the following discussion:

(i) Definition of QS states by (5.1). If small-scale components have large contributions to $|\dot{x}|$, defined QS patterns are irrelevant to quasi-stationary patterns in the real atmosphere. However, this contribution of small-scale components, such as (1, 3α) and (2, 3α) in our model, is small enough to be neglected compared with that of planetary-scale components; This is suggested by the first two rows in Table 4 which show the magnitude of $[|\dot{x}^n_m|]$ and $\sigma(|\dot{x}^n_m|)$ in the data used in Section 5.b. Here, $|\dot{x}^n_m|$ is defined as follows:

$$|\dot{x}^n_m| = \begin{cases} [(\dot{\psi}_{A_m})^2+(\dot{\theta}_{A_m})^2]^{1/2} & \text{for } n=0, \\ [(\dot{\psi}_{K^n_m})^2+(\dot{\psi}_{L^n_m})^2+(\dot{\theta}_{K^n_m})^2+(\dot{\theta}_{L^n_m})^2]^{1/2} & \text{for } n\neq 0. \end{cases} \tag{8.1}$$

(ii) Horizontal scale of MPs. In a barotropic model with 110 components, Yoden(1985) obtained several stationary solutions in which planetary-scale components dominate. Thus, the existence of MPs with dominant planetary-scale components would not be influenced by the existence of small-scale components.

(iii) Definition of *distance*. If small-scale components have large contributions to the definition of *distance*, the classification of each QS state according to the nearest MP in phase space becomes impossible. However, their contributions are also small enough to be neglected; This is implied by the last two rows in Table 4 which show the magnitude of $[|x^n_m|]$ and $\sigma(|x^n_m|)$ in the data used in Section 5.b. Here, $|x^n_m|$ is defined as follows:

$$|x^n_m| = \begin{cases} [(\psi_{A_m})^2+(\theta_{A_m})^2]^{1/2} & \text{for } n=0, \\ [(\psi_{K^n_m})^2+(\psi_{L^n_m})^2+(\theta_{K^n_m})^2+(\theta_{L^n_m})^2]^{1/2} & \text{for } n\neq 0. \end{cases} \tag{8.2}$$

Moreover, we find that the neglect of components (2, 2α) and (1, 3α) in the definition of *distance* in Section 5.b has little effect on this definition.

Since the concept of quasi-stationary states has not been established, any observational research on the quasi-stationary patterns in the real atmosphere which can be compared with our model results has not been proceeded as yet. Therefore, it is interesting to analyze the quasi-stationary patterns in the real atmosphere by using our definition of QS states based on $|\dot{x}|$.

9. Conclusion

Dynamics and statistics of "quasi-stationary (QS)" states in irregular motions were investigated by using a two-layer, quasi-geostrophic spectral model in a mid-latitude β-channel with 28 retained components. A surface topography with zonal wavenumber 3, an external thermal forcing and dissipative processes were included in this model. We defined each QS state as a period when the magnitude of the time-derivative of the trajectory in phase space $|\dot{x}|$ is smaller than a prescribed threshold value. The following results were obtained;

(1) For a wide range of parameter values of the thermal forcing, each QS state occurs when the trajectory $x(t)$ passes in the vicinity of a local minimum point (MP) of $|\dot{x}|$ in phase space. The statistical significance of this relation between each QS state and an MP is obtained almost independent of the threshold value defining QS states.

(2) The MP is either a stationary solution or a non-stationary minimum point bifurcating from a limit point of a stationary solution. The latter point is the "ghost" equilibrium suggested by Legras and Ghil(1985). The bifurcation theory of stationary solutions can be generalized into that of MPs.

(3) The classification of each QS state according to the nearest MP in phase space reveals that some MPs are preferably selected to generate QS states independent of initial conditions. This selection is not due to the local dynamical property of each MP, such as the number and magnitude of the unstable eigenvalue of the MP, but is attributed to an inhomogeneous probability density distribution of trajectories in phase space.

(4) Probability that a QS state persists over n days is well expressed

as $\exp(-n/\tau)$, where τ is the characteristic time depending on each MP generating QS states. This probability distribution is also analytically deduced in a simple linearized system around an MP, which supports the relation between each QS state and an MP

(5) The prominent linear growth of an unstable eigenmode of the nearest MP is detected at the end of some QS states. This is a dynamical consequence of the relation between each QS state and the corresponding MP. On the other hand, the access of the trajectory on a stable eigenmode into the nearest MP at the beginning of a QS state is hardly detected, because stable eigenmodes span high dimensional sub-space.

We can apply our new concept of QS states to any dynamical systems and even to the real atmosphere. However, whether obtained QS states have any physical significance or not depends on their recurrent features which must be connected with the dynamics of the system, such as MPs. Therefore, before applying the concept of QS states to the recurrent quasi-stationary features in the real atmosphere, it is necessary to reexamine the relation between each QS state and an MP in less truncated mechanistic models and GCMs for the next study.

Acknowledgements

This work is a part of my doctoral dissertation submitted to Kyoto University in 1987. I would like to thank Profs. I. Hirota and S. Yoden for their continuing guidance and encouragement through my dissertation work. Thanks are also due to Profs. T. Iwashima and H. Fujii for their helpful suggestions about the bifurcation theory and numerical procedures to obtain stationary solutions. I also acknowledge stimulating discussions with Dr. J.-I. Yano.

The computations were performed on the FACOM M780/VP-200 computer at the Data Processing Center of Kyoto University.

APPENDIX A

Motions in the vicinity of an MIN

If $|\dot{x}|$ at an MIN is small enough to be neglected, which is the case of $\theta_A^*=0.054$ (see Table 1), the linearized equation around an MIN well represents the motions in the vicinity of the MIN. The linearized equation for the deviation field x' from the MIN is written as

$$\dot{x}' = Jx' \tag{A.1}$$

where J is the Jacobian of (3.2). From (3.1), we find that J has a zero-eigenvector, of which adjoint eigenvector is parallel to $\dot{x}$ at the MIN. In this linearized system, x' on the sub-space spanned with stable (unstable) eigenvectors of the MIN is attracted to (repelled from) the MIN, but there is no motion on the zero-eigenvector. We illustrate a simple example of a system $(\dot{x}, \dot{y})=(-\lambda-x^2, -y)$ (Fig.A1-a), of which linearized motion around the MIN (the origin) is shown in Fig.A1-(b).

APPENDIX B

Probability of the occurrence of a QS state in the linearized system around an MP

If we assume that (i) the motion is governed by the linearized equation (A.1) around an MP, (ii) QS states are defined when the deviation x' from the MP exists in the inside of a surface $|\dot{x}'|=C_0$, and (iii) x' is isotropically placed on that surface, *i.e.*, each angle θ^1, θ^2, ···, $\theta^{\nu-1}$ of $x'=(r, \theta^1, \theta^2, \cdots, \theta^{\nu-1})$ in the ν-dimensional polar coordinate is given at random at an initial time, the probability of the occurrence of a QS state is calculated by using the following Monte Carlo method.

The condition of the occurrence of a QS state for x'_i (subscript i denotes a trial number) is given by $(\nabla|\dot{x}'_i|^2 \cdot \dot{x}'_i)<0$ where $\nabla|\dot{x}'_i|^2$ and $\dot{x}'_i$ are calculated by using J of (3.2). Moreover, the direction of these two vectors is independent of r, *i.e.*, C_0. Therefore, the calculation on the surface $|\dot{x}'|=C_0$ is replaced with that on the ν-dimensional sphere (r=constant) (see Fig.B1). Thus, the probability P of the occurrence of a QS state is given by

$$P = \frac{\sum_i p_i W_i}{\sum_i W_i} \tag{B.1}$$

where

$$p_i = \begin{cases} 1 & if\ (\nabla|\dot{x}'_i|^2 \cdot \dot{x}'_i)<0 \\ 0 & if\ (\nabla|\dot{x}'_i|^2 \cdot \dot{x}'_i)>0 \end{cases}$$

and

$$W_i = \sin^{\nu-2}\theta_i^1 \ \sin^{\nu-3}\theta_i^2 \cdots \sin\theta_i^{\nu-2}$$

Equation (B.1) corresponds to an area mean of p_i on the ν-dimensional sphere. Here, we must increase the trial number i to obtain a precise

value of the probability.

Some modifications are necessary in the above calculation for an MIN because J has a zero eigenvector: (i) Rotate ν-dimensional rectangular-coordinate such that one coordinate becomes parallel to the zero eigenvector. (ii) Convert other $\nu-1$ coordinates into the polar coordinate $(r, \theta^1, \cdots, \theta^{\nu-2})$. (iii) Calculate (B.1) on this $\nu-1$ dimensional sphere.

We use the arbitrary precision mode in REDUCE 3 (the precision is 250 decimal digits) instead of FORTRAN (the precision is about 33 decimal digits), because FORTRAN cannot cover the range of the value of W_i in (B.1). The probability for S1 is 0.999··· (9 continues down to 67 places of decimals), and that for S2 is accurately 1.0 (0 continues down to 250 places of decimals) with 10 trial numbers; the trial numbers are limited because of the slowness in calculation by REDUCE 3. If we use FORTRAN, we can increase the trial numbers; we obtained the same result P=1.0 for a trial number of 10000.

We can deduce that *all* MPs at θ_λ^*=0.054 have the probability of almost 1.0, because each MP has a similar instability property to S1 (see Table 1).

APPENDIX C

Duration of QS states in a simple linearized system

Let us consider a simple linearized system:

$$(\dot{x},\ \dot{y})=(-ax,\ by) \tag{C.1}$$

as shown in Fig.C1. We define a QS state in this system as a period when $|\dot{x}|=(a^2x^2+b^2y^2)^{1/2}\leq C_0$. The probability that a QS state persists over a time t corresponds to the distribution of the duration time t when we give the initial condition $(x_0,\ y_0)=(r_0\cos\theta_0,\ r_0\sin\theta_0)$ on the ellipsoid $|\dot{x}|^2=a^2x^2+b^2y^2=C_0^2$ independent of θ_0. The relation between the duration time t and θ_0 is given by

$$\theta_0 = \arctan\left[\frac{a}{b}\left(\frac{1-e^{-2at}}{e^{2bt}-1}\right)^{1/2}\right], \tag{C.2}$$

which is independent of C_0. Therefore, if $0<\theta<\theta_0$, a QS state persists over a time t at least. Thus, the probability that a QS state persists over a time t is given by θ_0/θ_q where $\theta_q=\arctan(a/b)^{3/2}$; the duration time t is zero at $\theta=\theta_q$. This probability distribution is shown by the solid line in Fig.C2. Moreover, the asymptotic behavior of θ_0/θ_q in the limit of $t\to\infty$ is expressed as $\theta_0/\theta_q\to e^{-bt}$, which is the broken line in Fig.C2. Finally, the probability of the occurrence of a QS state in this system is given by $2\theta_q/\pi$.

REFERENCES

Cehelsky, P., and K. K. Tung, 1987: Theories of multiple equilibria and weather regimes – A critical reexamination. Part I: Baroclinic two-layer models. To be appeared in *J. Atmos. Sci.*

Charney, J. G., and J. G. DeVore, 1979: Multiple flow equilibria in the atmosphere and blocking. *J. Atmos. Sci.*, 36, 1205–1216.

Dole, R. M., 1983: Persistent anomalies of the extratropical Northern Hemisphere wintertime circulation. *Large-scale Dynamical Processes in the Atmosphere*, B. J. Hoskins and R. P. Pearce, Eds., Academic Press, 95–109.

Ghil, M., and S. Childress, 1987: *Topics in Geophysical Fluid Dynamics: Atmospheric Dynamics, Dynamo Theory, and Climate Dynamics.* Springer-Verlag, New York, 485pp.

Hartmann, D. L., and S. J. Ghan, 1980: A statistical study of the dynamics of blocking. *Mon. Wea. Rev.*, 108, 1144–1159.

Iwashima, T., and R. Yamamoto, 1986: Time-space spectral general circulation model. I. Time-space spectral model of low-order barotropic system with periodic forcing. *J. Meteor Soc. Japan*, 64, 183–196.

Kubíček, M., and M. Marek, 1983: *Computational Methods in Bifurcation Theory and Dissipative Structures.* Springer-Verlag, New York, 243pp.

Legras, B., and M. Ghil, 1985: Persistent anomalies, blocking and variations in atmospheric predictability. *J. Atmos. Sci.*, 42, 433–471.

Mo, K. C., and M. Ghil, 1987a: Statistics and dynamics of persistent anomalies. *J. Atmos. Sci.*, 44, 877–901.

———, and ———, 1987b: Cluster analysis of multiple planetary flow regimes. Submitted to *J. Geophys. Res.*

Mukougawa, H., 1987: Instability of topographically forced Rossby waves in a two-layer model. *J. Meteor. Soc. Japan*, 65, 13-25.

Reinhold, B. B., and R. T. Pierrehumbert, 1982: Dynamics of weather regimes: quasi-stationary waves and blocking. *Mon. Wea. Rev.*, 110, 1105-1145.

———, and ———, 1985: Corrections to "Dynamics of weather regimes: quasi-stationary waves and blocking" *Mon. Wea. Rev.*, 113, 2055-2056.

Yoden, S., 1983: Nonlinear interactions in a two-layer, quasi-geostrophic, low-order model with topography. Part I: Zonal flow-forced wave interactions. Part II: Interactions between zonal flow, forced waves and free waves. *J. Meteor Soc. Japan*, 61, 1-35.

———, 1985: Multiple stable states of quasi-geostrophic barotropic flow over sinusoidal topography. *J. Meteor Soc. Japan*, 63, 1031-1045.

TABLE 1. Some dynamical properties of all MPs at θ_A^*=0.054. Couples of MPs having same dynamical properties are listed in same rows. φ_{A_1} denotes the most gravest barotropic zonal component and $|\dot{x}|$ is the magnitude of the time-derivative of spectral components at MP. All unstable eigenvalues for each MP are listed in the fourth column. The imaginary unit is denoted by i. MS1 and MS2 consist of innumerable points having different stability characteristics, respectively.

MP	φ_{A_1}	$\lvert\dot{x}\rvert$	unsatble eigenvalue		
S1	0.0379	0.0	0.033±0.035i	0.007±0.043i	0.007
S2, S3	0.0304	0.0	0.017±0.040i	0.000±0.026i	
M1 M2	0.0355	1.6×10^{-5}	0.024±0.054i		
M3, M4	0.0303	2.6×10^{-5}	0.020±0.037i	0.010	
M5, M6	0.0264	3.3×10^{-5}	0.043		
M7, M8	0.0232	1.1×10^{-5}	0.010±0.032i		
M9, M10	0.0222	1.6×10^{-5}	0.017±0.050i	0.018±0.036i	
M11 M12	0.0179	1.5×10^{-5}	0.016±0.052i	0.001±0.056i	
M13, M14	0.0095	4.9×10^{-5}	0.027±0.066i	0.006±0.028i	
MS1	0.0216	1.4×10^{-5}			
MS2	0.0033	1.5×10^{-4}			

TABLE 2. Classification of QS states in a 2000-day record with asymptotic behavior in each time integration from the initial value (a), (b), ···· (n) at $\theta_\lambda^\dagger$=0.054. (a) M1; (b) M3; (c) M5; (d) M7; (e) M9; (f) one point of MS1; (g) M11; (h) M13; (i) one point of MS2; (j) S1 + its unstable mode of the largest growth rate; (k) S1 + its unstable mode of the second largest growth rate; (l) S1 + its unstable mode of the smallest growth rate; (m) S2 + its unstable mode of the largest growth rate; (n) S2 + its unstable mode of the smallest growth rate. Note that integrations from S3, M2, M4, ···, M14 have not been proceeded by taking account of the dynamical properties in this system discussed in Section 2.c. For example, let us consider two data sets generated by the integration from M1 and M2. Then, the following properties are found: (i) two data sets are identical to each other except for the sign of T-mode components; (ii) all the same QS states are defined in these two data sets; (iii) the nearest MPs during the corresponding QS state in these two data sets are converted into each other by the transformation T of (2.15), such as S2 and S3.

Initial value	S1	S2 S3	M1 M2	M3 M4	M5 M6	M7 M8	M9 M10	M11 M12	M13 M14	MS1	MS2
(a)	0	11	0	8	0	3	0	1	0	8	0
(b)	1	15	2	5	1	5	0	2	0	2	0
(c)	2	12	0	7	0	2	0	1	0	7	0
(d)	1	11	1	5	0	4	1	0	0	7	0
(e)	0	15	0	9	0	4	0	0	0	2	0
(f)	1	12	1	5	0	3	0	1	0	7	0
(g)	1	15	1	5	2	3	0	0	0	6	0
(h)	1	13	0	5	0	5	0	0	0	0	0
(i)	0	20	0	1	0	4	0	0	0	5	0
(j)	1	21	1	5	0	3	0	0	0	4	0
(k)	0	14	4	5	0	7	0	1	0	12	0
(l)	1	10	0	4	0	9	1	0	0	6	0
(m)	1	3	0	4	1	4	0	0	0	6	0
(n)	1	17	2	5	2	4	0	0	0	4	0
Total	11	189	12	73	6	60	2	6	0	76	0

TABLE 3. Characteristics of the attractor basin of each MP at $\theta_A^{\dagger}$=0.054. All data sets in Table 2 are used to calculate each quantity. Each day is classified according to the nearest MP in phase space, and the total days of each group are listed in the second column. Total days of each group of QS states classified by the nearest MP are listed in the third column. Maximum and minimum *distance* from each MP in the corresponding group of QS (non-QS) states are listed in the fourth and fifth (sixth and seventh) columns.

MP	Proximity (day)	QS (day)	Distance ($\times 10^{-4}$) QS max.	QS min.	non-QS max.	non-QS min.
S1	272	52	175	107	209	100
S2 S3	8437	1236	235	62	289	67
M1 M2	1925	36	227	108	249	95
M3. M4	3393	439	235	62	282	68
M5. M6	909	21	164	129	312	78
M7, M8	3117	367	205	60	304	75
M9. M10	2511	5	223	152	292	90
M11 M12	1097	37	206	113	298	89
M13, M14	31	0	—	—	304	128
MS1	6276	659	211	53	292	67
MS2	32	0	—	—	286	171

TABLE 4. Mean value (Mean) and standard deviation (Std. Dev.) of $|\dot{x}_m^n|$ (multiplied by 10^6) and $|x_m^n|$ (multiplied by 10^4) for the 5000-day record used in Section 5.b at $\theta_\lambda^*=0.054$.

(m, nα)		(1 0)	(2, 0)	(1 α)	(2, α)	(1 2α)	(2, 2α)	(1 3α)	(2, 3α)
$\lvert\dot{x}_m^n\rvert$	Mean	117	192	204	287	300	203	121	73
	Std. Dev	79	157	130	154	217	84	60	44
$\lvert x_m^n\rvert$	Mean	432	58	76	115	100	91	30	15
	Std. Dev	40	35	27	42	50	36	13	7

FIGURE CAPTIONS

Fig.1. Schematic diagram of the two-layer model.

Fig.2. Schematic diagram of some critical points of an MIN. Two axes λ and x are the bifurcation parameter and a dependent variable in the system, respectively. Solid line is an MIN branch and broken line is a saddle point branch. Critical point is indicated by X. (a) "limit point". (b) super-critical "bifurcation point". (c) sub-critical "bifurcation point"

Fig.3. Schematic diagram of the bifurcation of an MIN from a critical point of a stationary solution for two illustrative examples. (a) Limit point: $(\dot{x}, \dot{y})=(\lambda-x^2, y)$. (b) Bifurcation point: $(\dot{x}, \dot{y})=(x^3-\lambda x, y)$. λ is the bifurcation parameter. Thick solid line is a stationary solution branch, thin solid line is an MIN branch and broken line is a saddle point branch. Critical point is indicated by X.

Fig.4. Variation of $|\dot{\mathbf{x}}|$ on a segment in phase space which contains a stationary solution (S2) and an MIN (M7) at $\theta^*_\lambda=0.054$. The origin of the abscissa denotes S2 and 1 is M7.

Fig.5. Bifurcation diagram of stationary solutions (thick lines) and MINs (thin lines) for the external parameter θ^*_λ. The ordinate denotes φ_{A_k}. Two branches having the same dynamical properties are degenerated into one line. Some branches are named S1, ···, S5, M1, ···, M12, MS1. Stable (unstable) stationary solutions are indicated by the symbol s (u) on the branches. The bifurcation point of S1 is denoted by B, the first Hopf-bifurcation point of S2 and S3 by H and the limit point of S4 and S5 by L.

Fig.6. Stream function of all stationary solutions (S1, S2, S3) at $\theta^*_\lambda=0.054$. Surface topography is shown in right-bottom with negative region shaded.

Fig.7. Upper-layer stream function of all MINs (M1, M2, ···, M14) at θ_A^*=0.054. Stream function of one point of MS1 and MS2 is also shown.

Fig.8. Upper-layer stream function of S4 at its limit point at θ_A^*=0.0549.

Fig.9. Numerical solutions depending on θ_A^*. Temporal evolution of φ_{A_1} and its power spectral density of solutions (a, b, ···, e) are shown in Fig.10 and Fig.11, respectively.

Fig.10. Time evolution of φ_{A_1} component in some numerical solutions. The abscissa denotes the day from the beginning of the record with asymptotic behavior.

Fig.11. Power spectral density of φ_{A_1} variation shown in Fig.10. The abscissa denotes the frequency in cycle/day.

Fig.12. Time variation of $|\dot{x}|$ at θ_A^*=0.054. The horizontal solid line is $[|\dot{x}|]$ and the dotted line $[|\dot{x}|]-\sigma(|\dot{x}|)$. Each QS state is indicated by a vertical line whose width is its period.

Fig.13. Time variation of *distance* from the nearest MP (solid line) and that from the second-nearest MP (broken line) at θ_A^*=0.054 in the period of Fig.12. Each QS state is indicated by a vertical line whose width is its period.

Fig.14. Sequence of upper-layer stream function in a QS period which occurs in the vicinity of M8 for day 1210-1217 at θ_A^*=0.054.

Fig.15. (a) Variation of *distance* from the nearest MP in phase space against the threshold value for the definition of QS states at θ_A^*=0.054. (b) As in (a) except for *distance* from the second-nearest MP. The abscissa is C of that threshold value C_0 ($C_0=[|\dot{x}|]+C\sigma(|\dot{x}|)$) and the ordinate is *distance*. Solid lines are $[|DX_i|_{at\ t=t_m}]_{QS}$ and shaded regions are ranges of $[|DX_i|]_{non\text{-}QS}\pm\sigma(|DX_i|)_{non\text{-}QS}$, where i=1 for (a) and i=2 for (b). The definition of the above quantities is written in the text.

Fig.16. (a) Variation of *distance* from the nearest MP in phase space

against θ_A^*. (b) As in (a) except for *distance* from the second-nearest MP. The abscissa is θ_A^* and the ordinate is *distance*. Solid lines are $[|DX_i|_{at\ t=t_m}]_{QS}$ and shaded regions are ranges of $[|DX_i|]_{non\text{-}QS} \pm \sigma(|DX_i|)_{non\text{-}QS}$, where i=1 for (a) and i=2 for (b).

Fig.17 Persistence distribution of QS states in some groups occurring in the vicinity of the same MP at θ_A^*=0.054 (solid lines). All data sets in Table 2 are used. The ordinate is the total number of events which persist over n days on a *log*-scale and the abscissa is in days. Broken lines are computed using a least squares by $A\exp(-t/\tau)$. Each characteristic time τ is also presented.

Fig.18. Same as in Fig.12. The period of a QS state is denoted by two vertical lines.

Fig.19. Time variation of complex expansion coefficient of the most unstable eigenmode of S2 for the deviation field from S2 from day 4222 (denoted by S) to day 4236 (denoted by E) (solid line). The abscissa is the real part and the ordinate the imaginary part. Broken line shows the assumed linear growth of this eigenmode from day 4222. Small dots are plotted every two days from day 4222.

Fig.20. (a) Time variation of the upper-layer stream function of the deviation field from S2. (b) Time variation of the upper-layer stream function of the most unstable eigenmode of S2. Its amplitude is given by the expansion coefficient of this eigenmode for the deviation field.

Fig.21 (a) Time variation of the amplitude of the gravest barotropic wave component in the demonstration case of RP. (b) As in (a) except for the phase. (c) As in (a) except for $|\dot{x}|$. Each period of the weather regime is denoted by R (ridge) and T (trough). Each QS state is indicated by a vertical line whose width is its period.

Fig.A1. (a) Flows in $(\dot{x}, \dot{y})=(-\lambda-x^2, -y)$ (λ=0.1). (b) The linearized flows of (a) around the MIN (the origin). Stable and zero eigenvector of

the MIN is y-axis and x-axis, respectively.

Fig.B1. The direction of the vector $\nabla|\dot{x}'_i|^2$ and $\dot{x}'_i$ at a point (*e.g.*, a and b) on the surface of $|\dot{x}'_i|=C_0$ is identical to that at the corresponding point (*e.g.*, a' and b') on the ν-dimensional sphere (r=constant) for the linearized equation around an MP

Fig.C1. Schematic diagram of flows in $(\dot{x}, \dot{y})=(-ax, by)$. The ellipsoid $a^2x^2+b^2y^2=C_0^2$ is drawn by solid line.

Fig.C2. Probability that a QS state persists over a time t in the system of $(\dot{x}, \dot{y})=(-ax, by)$ (solid line). Broken line shows the asymptotic behavior, e^{-bt} in the limit of $t\to\infty$.

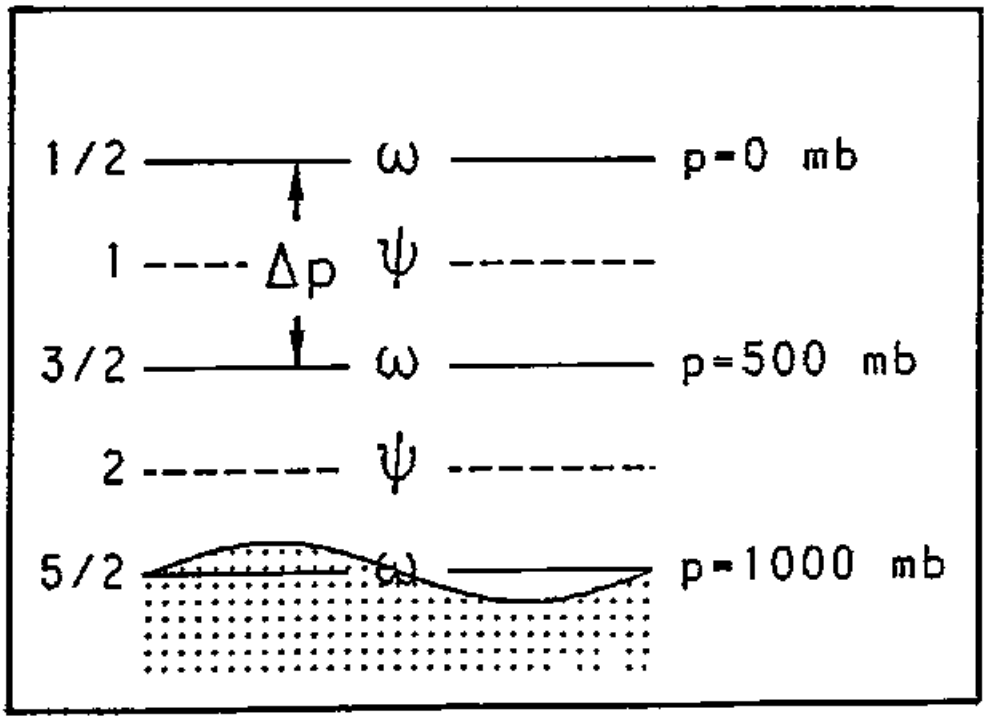

Fig.1. Schematic diagram of the two-layer model.

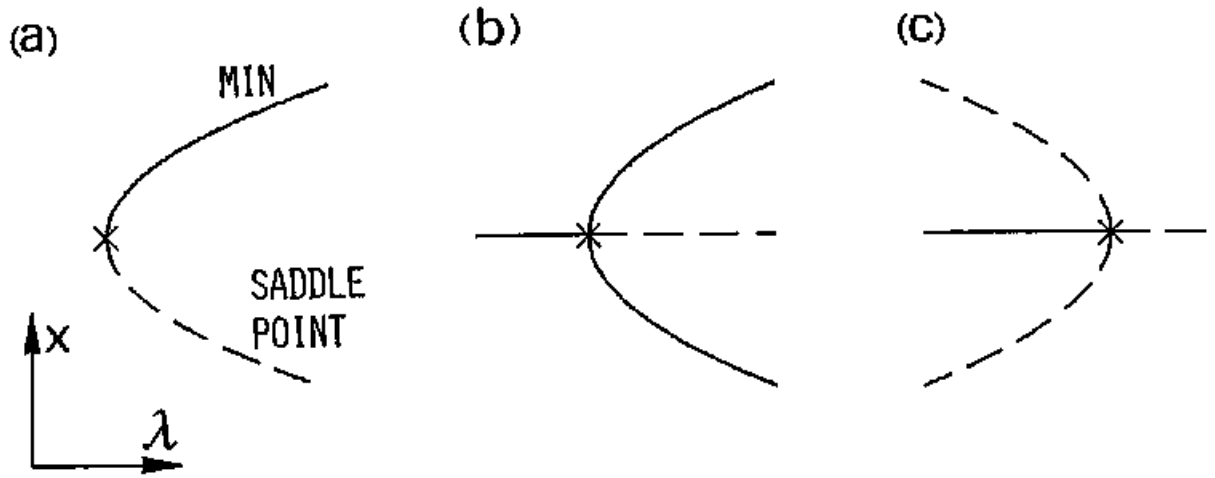

Fig.2. Schematic diagram of some critical points of an MIN. Two axes λ and x are the bifurcation parameter and a dependent variable in the system, respectively. Solid line is an MIN branch and broken line is a saddle point branch. Critical point is indicated by X. (a) "limit point" (b) super-critical "bifurcation point" (c) sub-critical "bifurcation point"

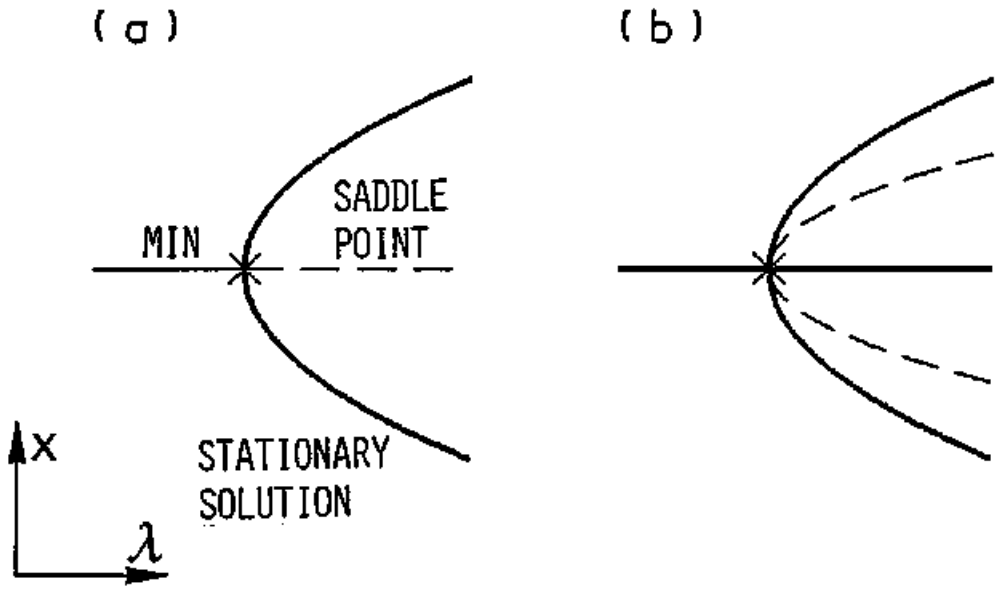

Fig.3. Schematic diagram of the bifurcation of an MIN from a critical point of a stationary solution for two illustrative examples. (a) Limit point: $(\dot{x}, \dot{y})=(\lambda-x^2, y)$. (b) Bifurcation point: $(\dot{x}, \dot{y})=(x^3-\lambda x, y)$. λ is the bifurcation parameter. Thick solid line is a stationary solution branch, thin solid line is an MIN branch and broken line is a saddle point branch. Critical point is indicated by X.

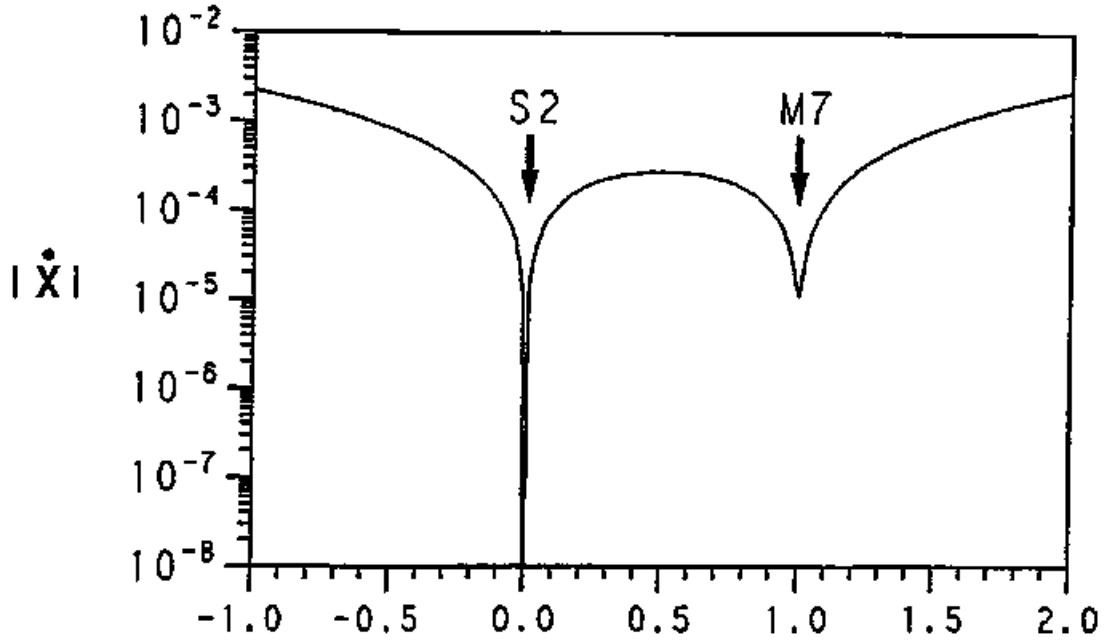

Fig.4. Variation of $|\dot{x}|$ on a segment in phase space which contains a stationary solution (S2) and an MIN (M7) at $\theta_A^*=0.054$. The origin of the abscissa denotes S2 and 1 is M7.

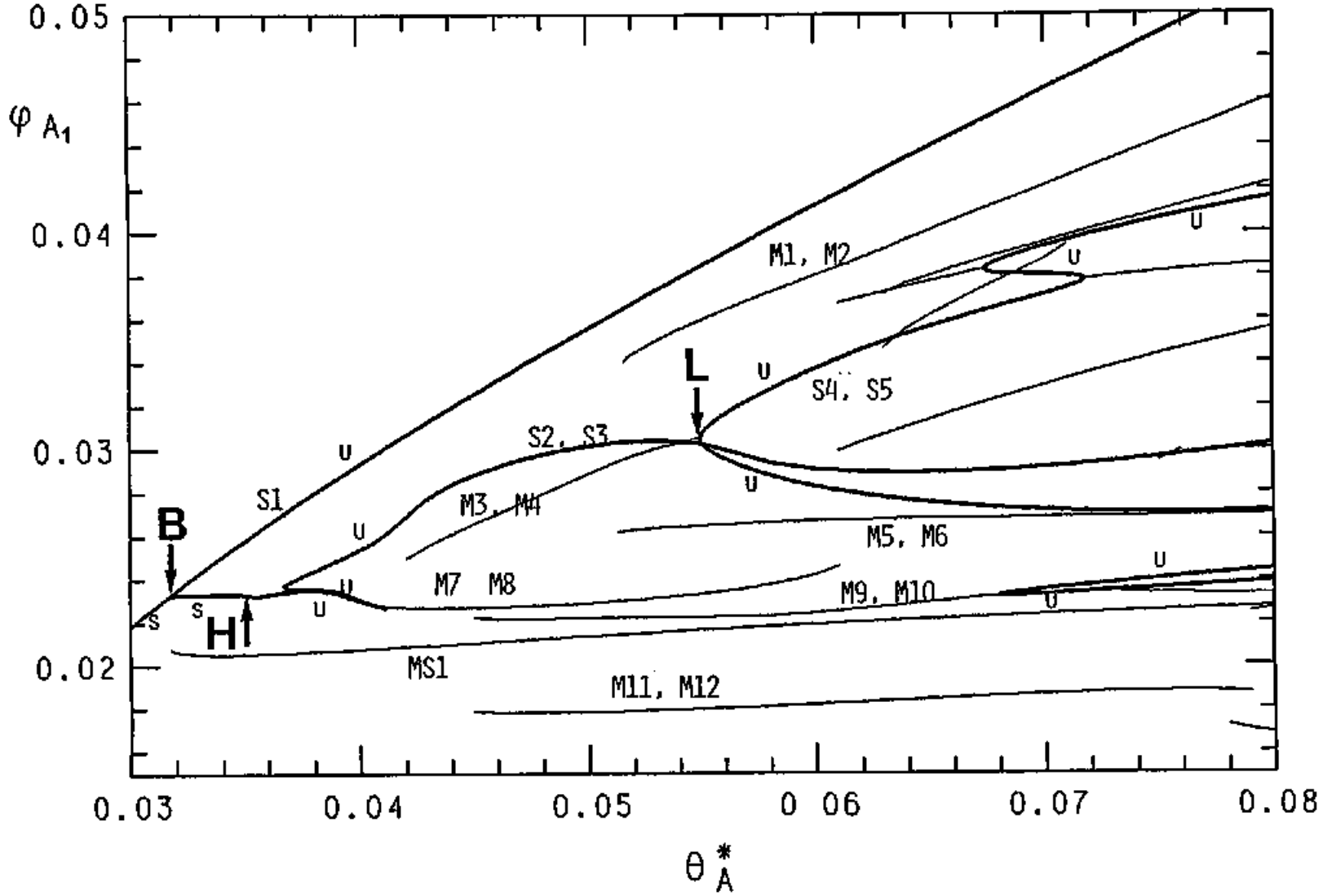

Fig.5. Bifurcation diagram of stationary solutions (thick lines) and MINs (thin lines) for the external parameter θ^*_A. The ordinate denotes φ_{A_1}. Two branches having the same dynamical properties are degenerated into one line. Some branches are named S1, ···, S5, M1, ···, M12, MS1. Stable (unstable) stationary solutions are indicated by the symbol *s* (*u*) on the branches. The bifurcation point of S1 is denoted by B, the first Hopf-bifurcation point of S2 and S3 by H and the limit point of S4 and S5 by L.

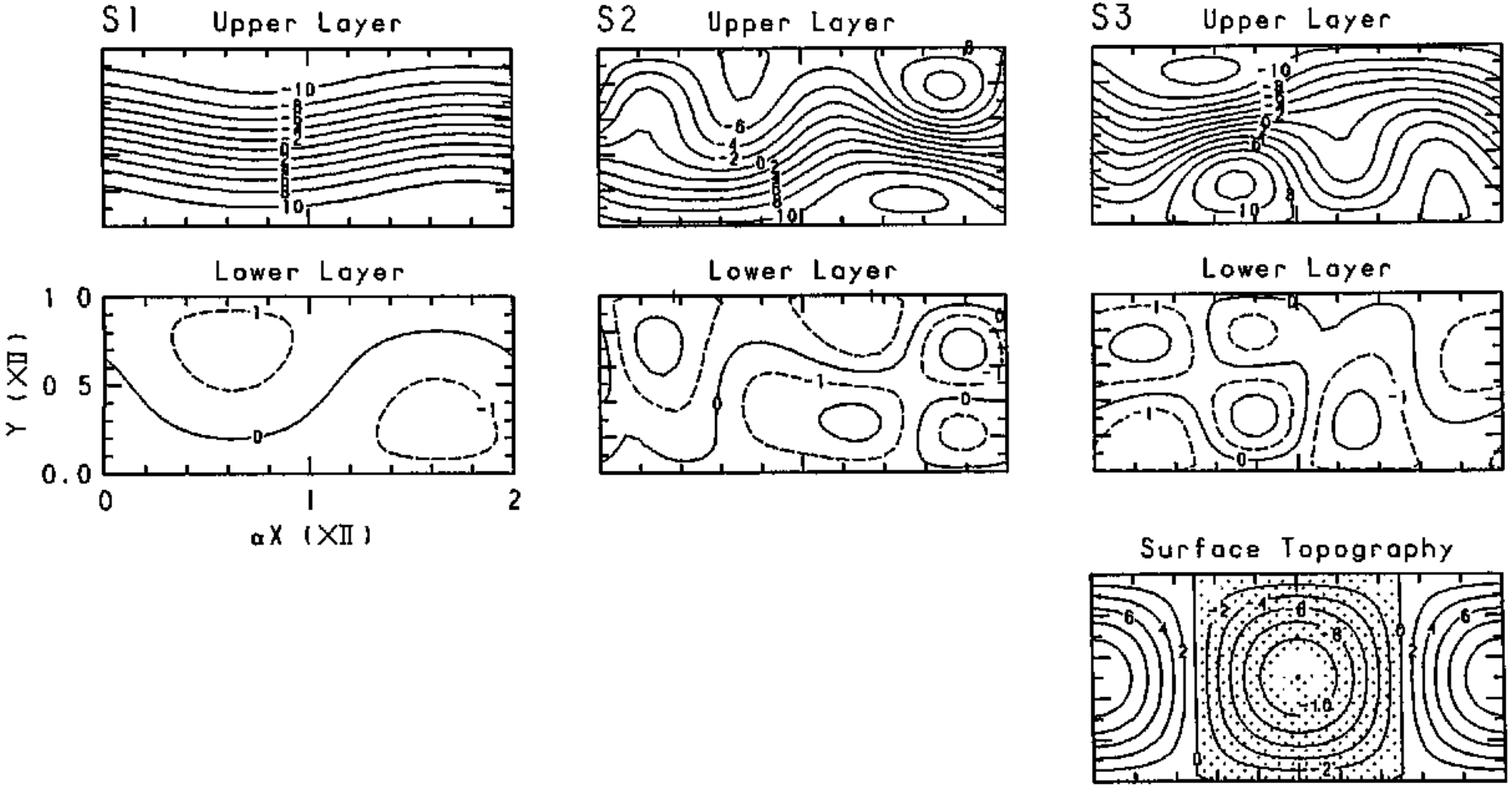

Fig.6. Stream function of all stationary solutions (S1, S2, S3) at θ_A^*=0.054.
Surface topography is shown in right-bottom with negative region shaded.

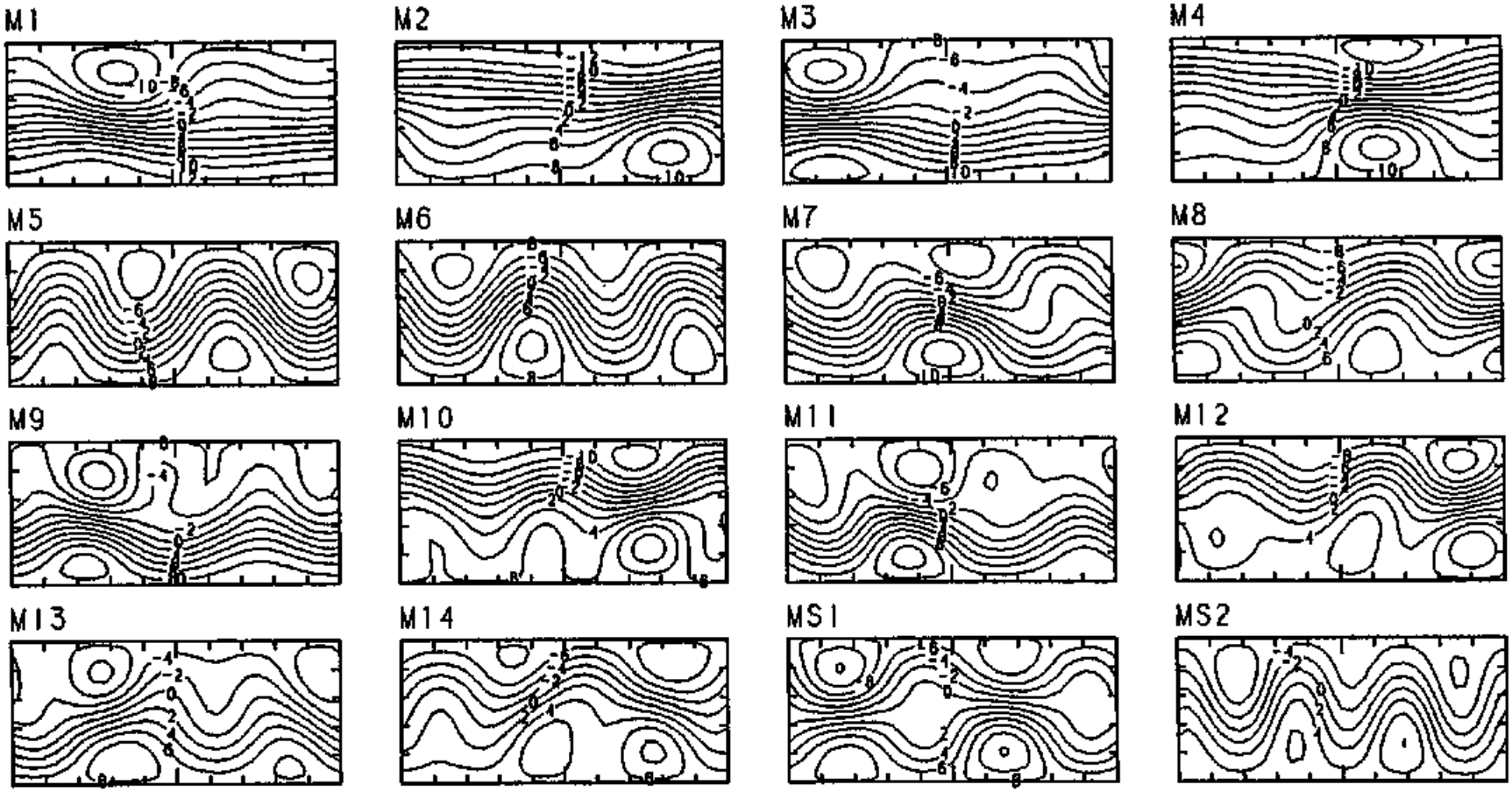

Fig.7. Upper-layer stream function of all MINs (M1, M2, ···, M14) at θ_A^*=0.054. Stream function of one point of MS1 and MS2 is also shown.

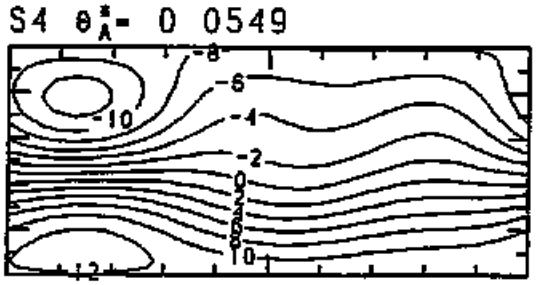

Fig.8. Upper-layer stream function of S4 at its limit point at θ_A^*=0.0549.

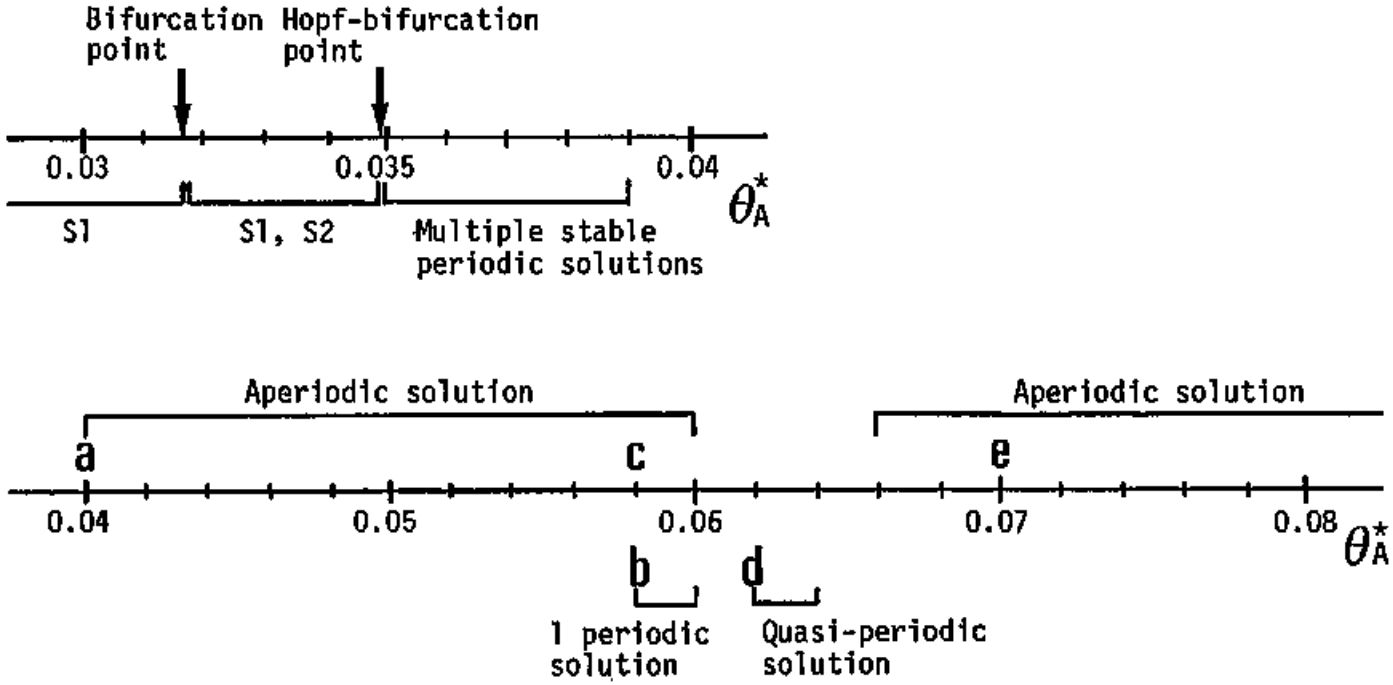

Fig.9. Numerical solutions depending on θ_A^*. Temporal evolution of φ_{A_1} and its power spectral density of solutions (a, b, ··· e) are shown in Fig.10 and Fig.11, respectively.

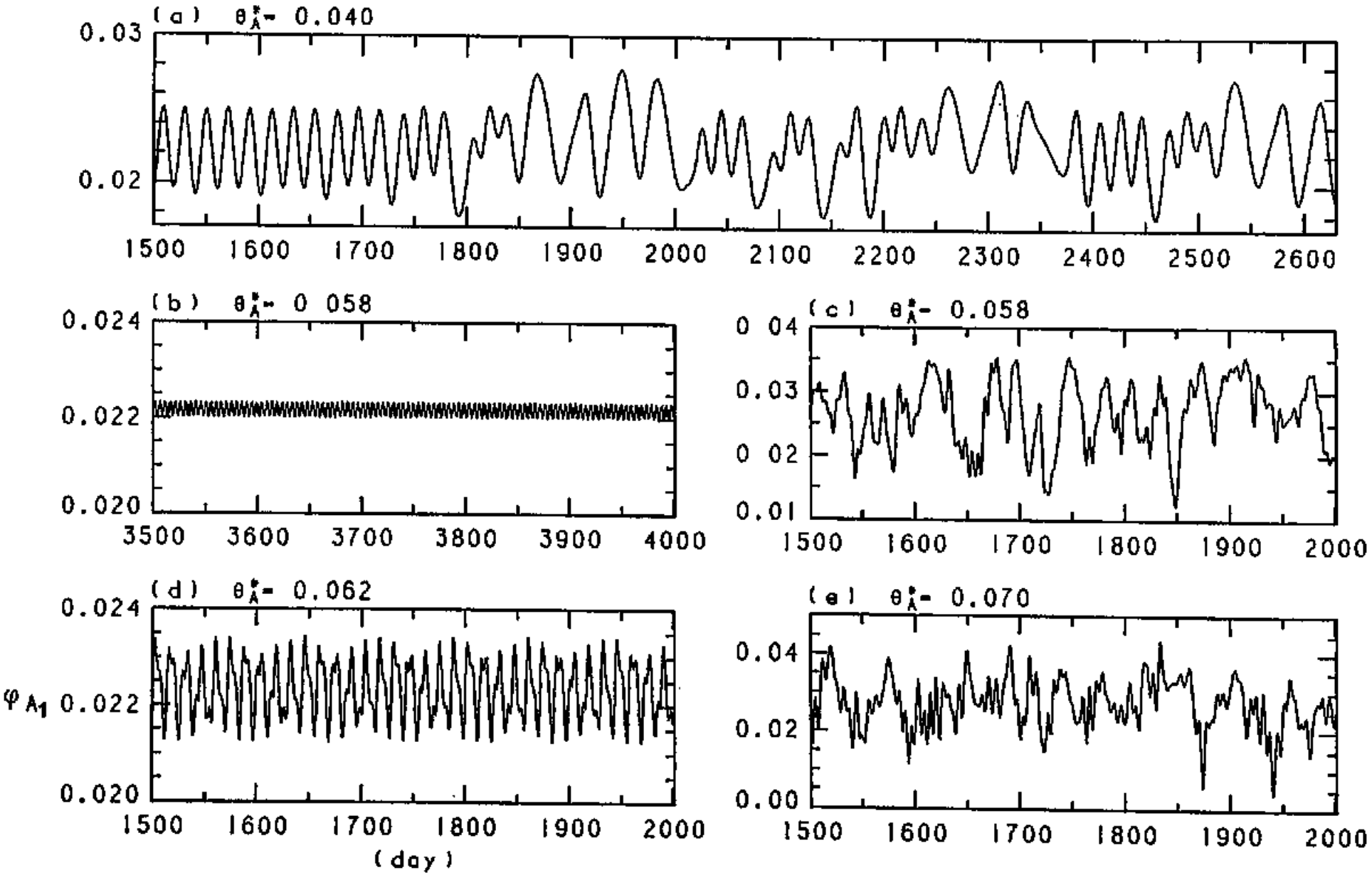

Fig.10. Time evolution of φ_{A_1} component in some numerical solutions. The abscissa denotes the day from the beginning of the record with asymptotic behavior.

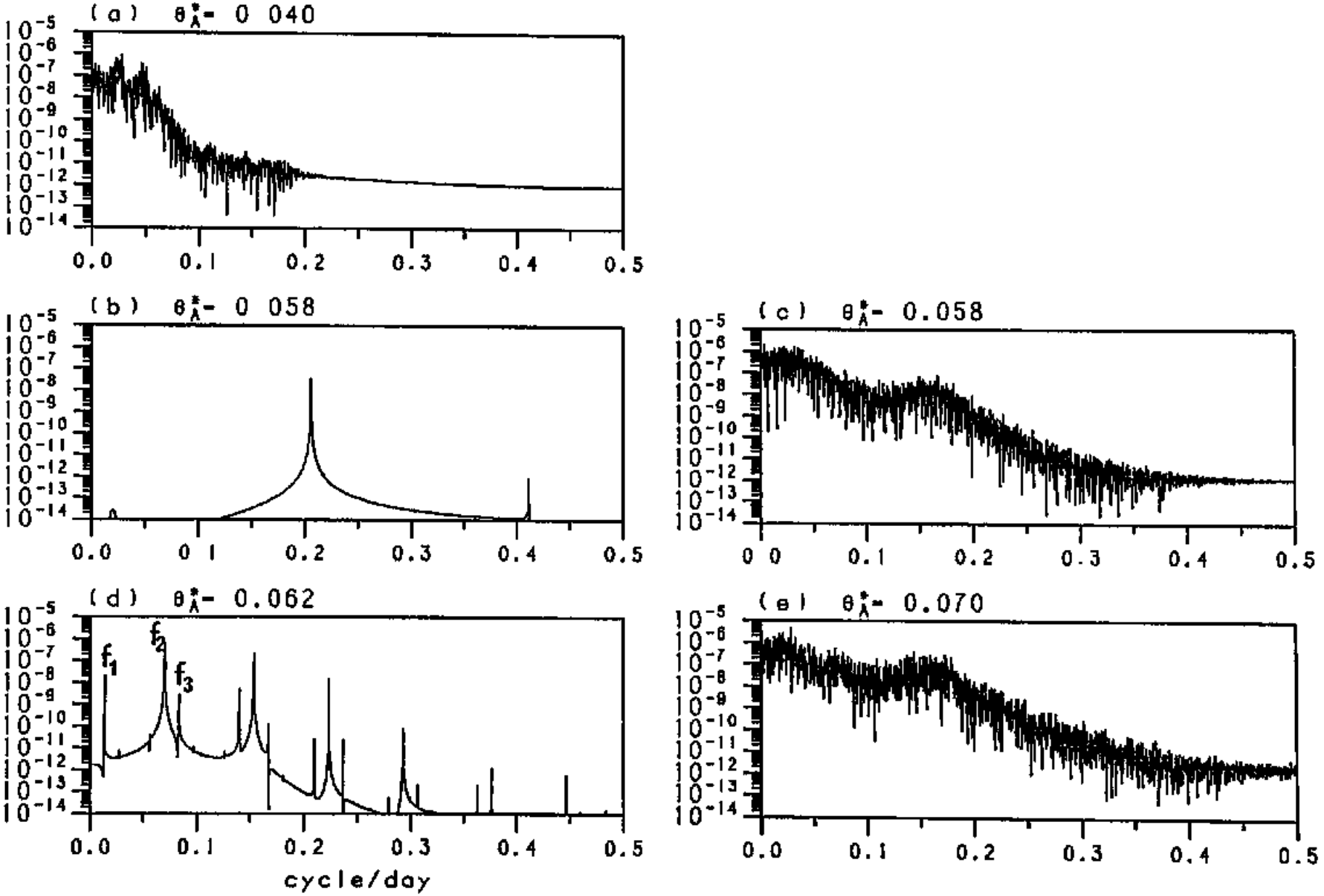

Fig.11. Power spectral density of φ_{A_1} variation shown in Fig.10. The abscissa denotes the frequency in cycle/day.

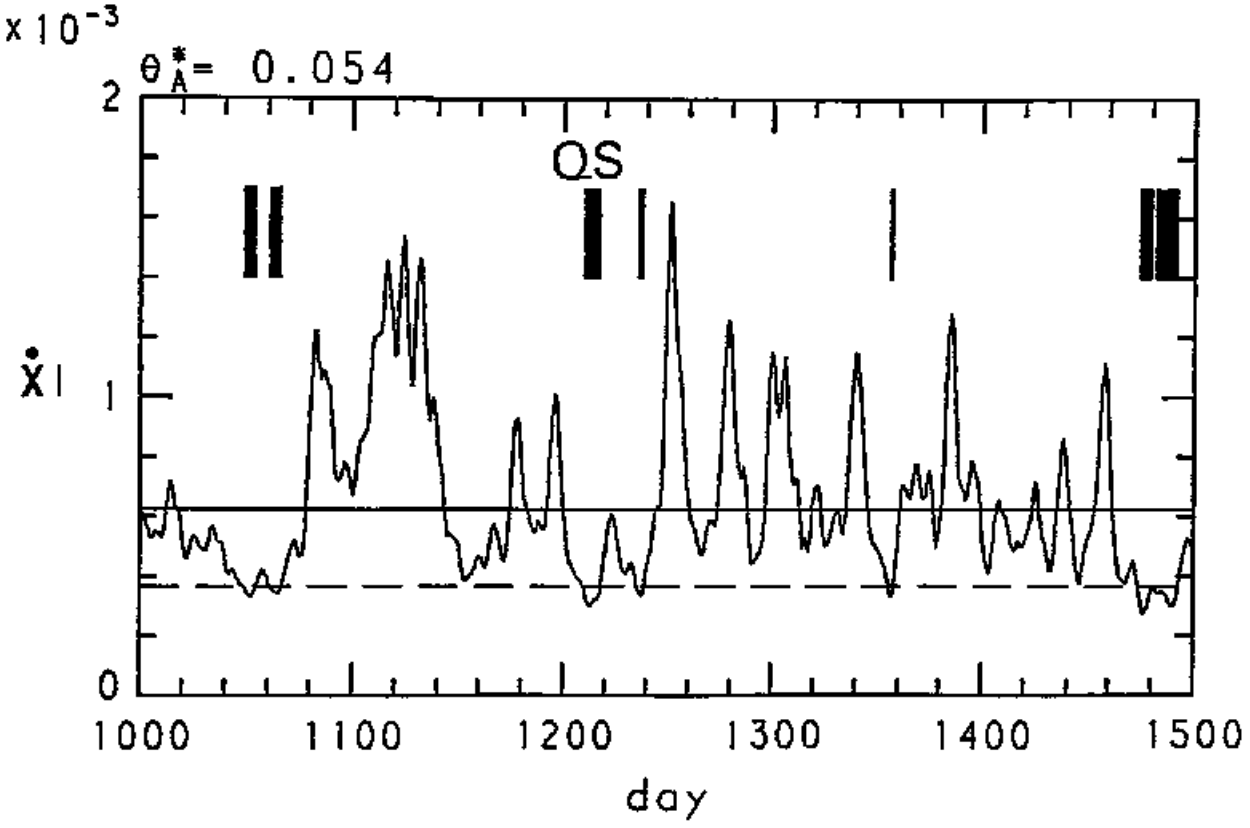

Fig.12. Time variation of $|\dot{x}|$ at θ_A^*=0.054. The horizontal solid line is $[|\dot{x}|]$ and the dotted line $[|\dot{x}|]-\sigma(|\dot{x}|)$. Each QS state is indicated by a vertical line whose width is its period.

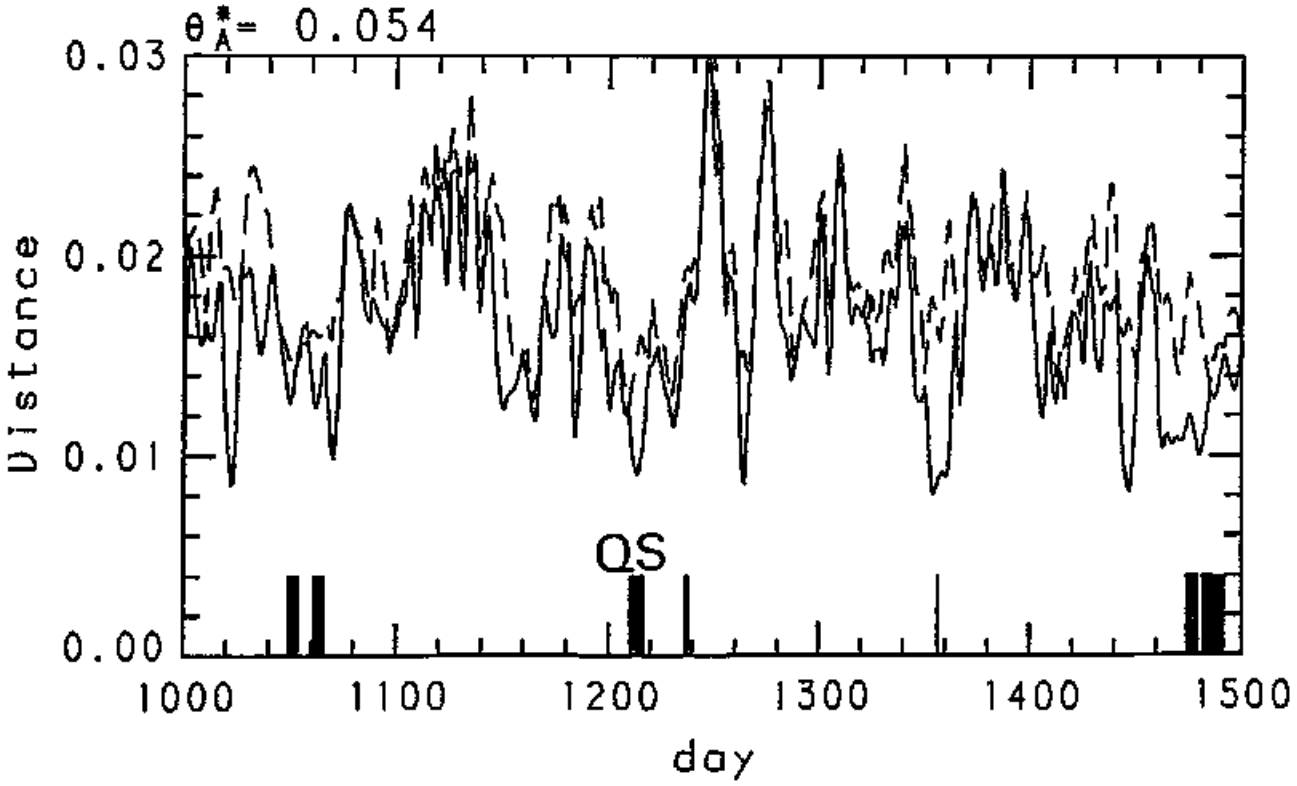

Fig.13. Time variation of *distance* from the nearest MP (solid line) and that from the second-nearest MP (broken line) at θ_A^*=0.054 in the period of Fig.12. Each QS state is indicated by a vertical line whose width is its period.

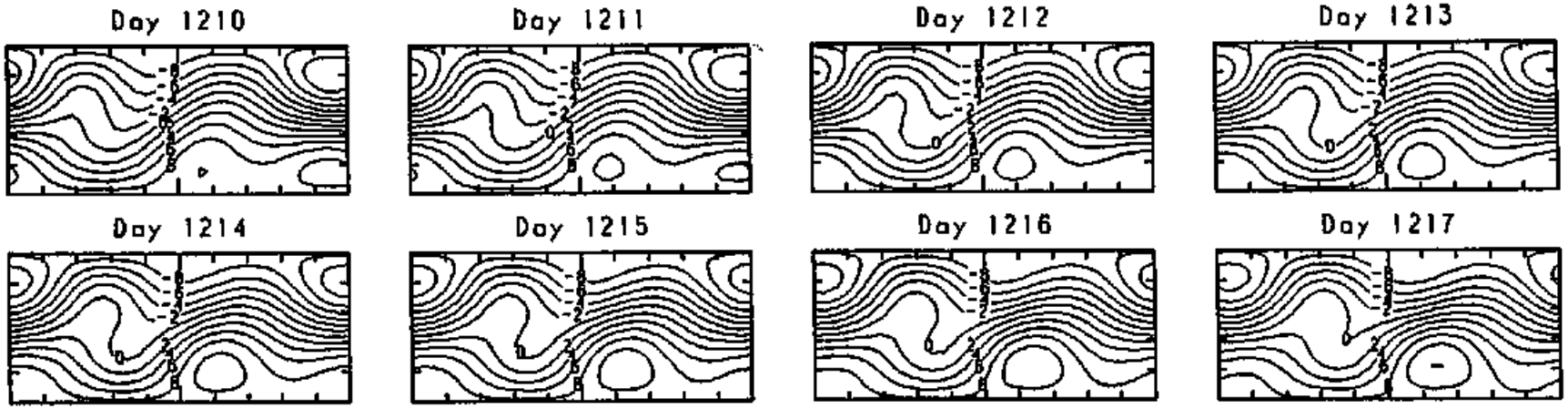

Fig.14. Sequence of upper-layer stream function in a QS period which occurs in the vicinity of M8 for day 1210-1217 at θ_1^*=0.054.

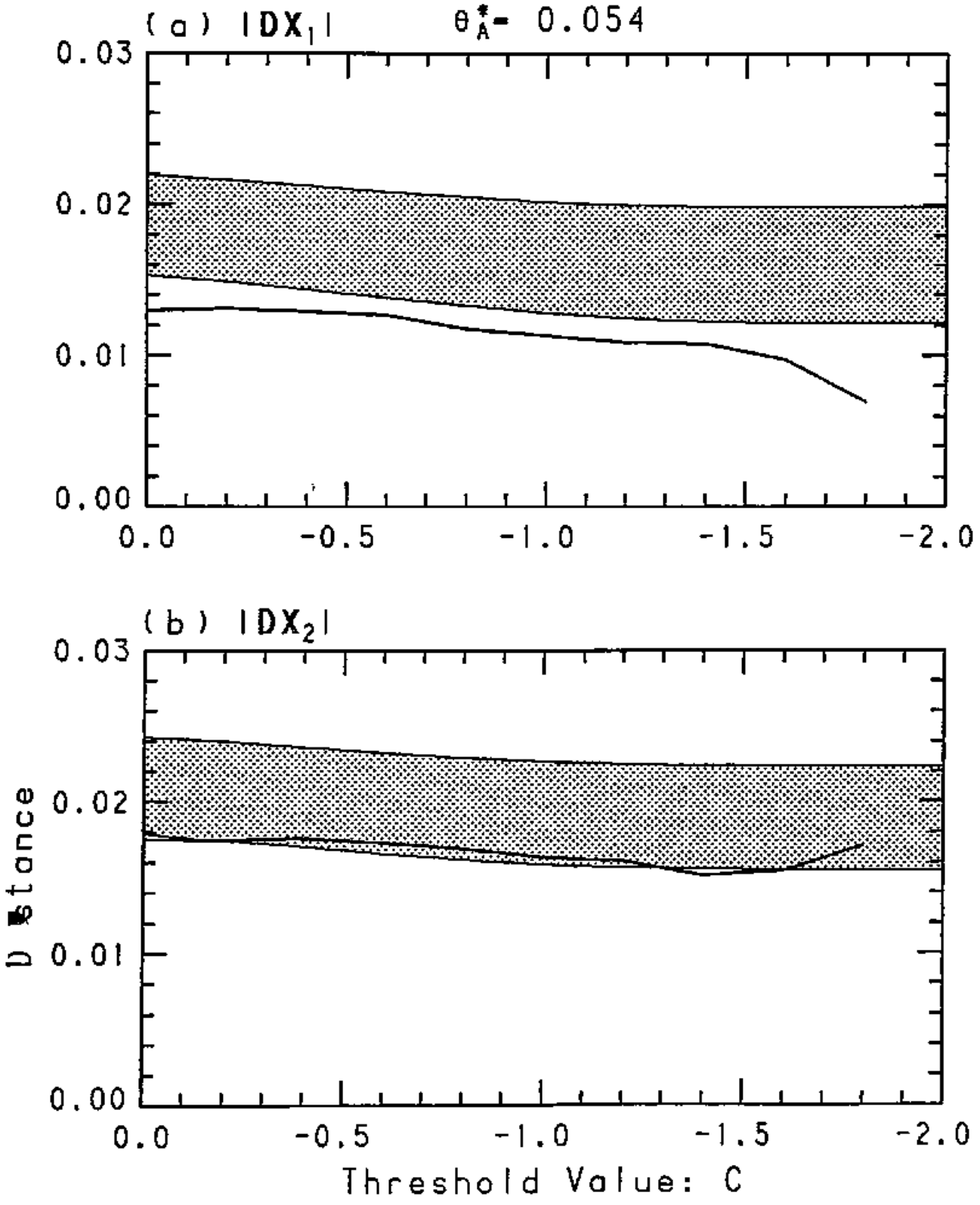

Fig.15. (a) Variation of *distance* from the nearest MP in phase space against the threshold value for the definition of QS states at θ_A^*=0.054. (b) As in (a) except for *distance* from the second-nearest MP. The abscissa is C of that threshold value C_0 ($C_0=[|\dot{x}|]+C\sigma(|\dot{x}|)$) and the ordinate is *distance*. Solid lines are $[|DX_i|_{at\ t=t_n}]_{QS}$ and shaded regions are ranges of $[|DX_i|]_{non\text{-}QS}\pm\sigma(|DX_i|)_{non\text{-}QS}$, where i=1 for (a) and i=2 for (b). The definition of the above quantities is written in the text.

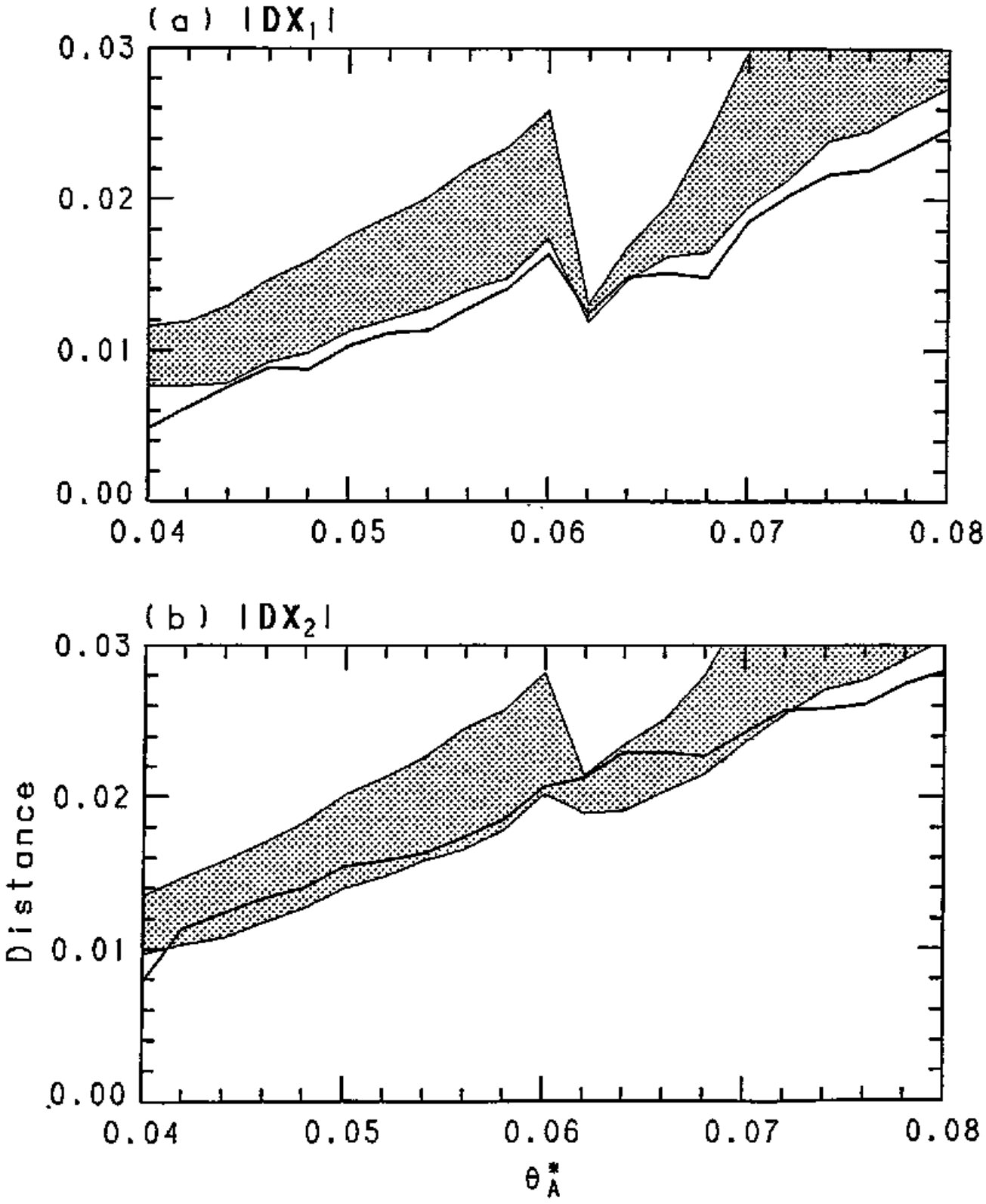

Fig.16. (a) Variation of *distance* from the nearest MP in phase space against θ_A^*. (b) As in (a) except for *distance* from the second-nearest MP. The abscissa is θ_A^* and the ordinate is *distance*. Solid lines are $[|DX_i|_{\text{at } t=t_n}]_{QS}$ and shaded regions are ranges of $[|DX_i|]_{\text{non-QS}} \pm \sigma(|DX_i|)_{\text{non-QS}}$, where i=1 for (a) and i=2 for (b).

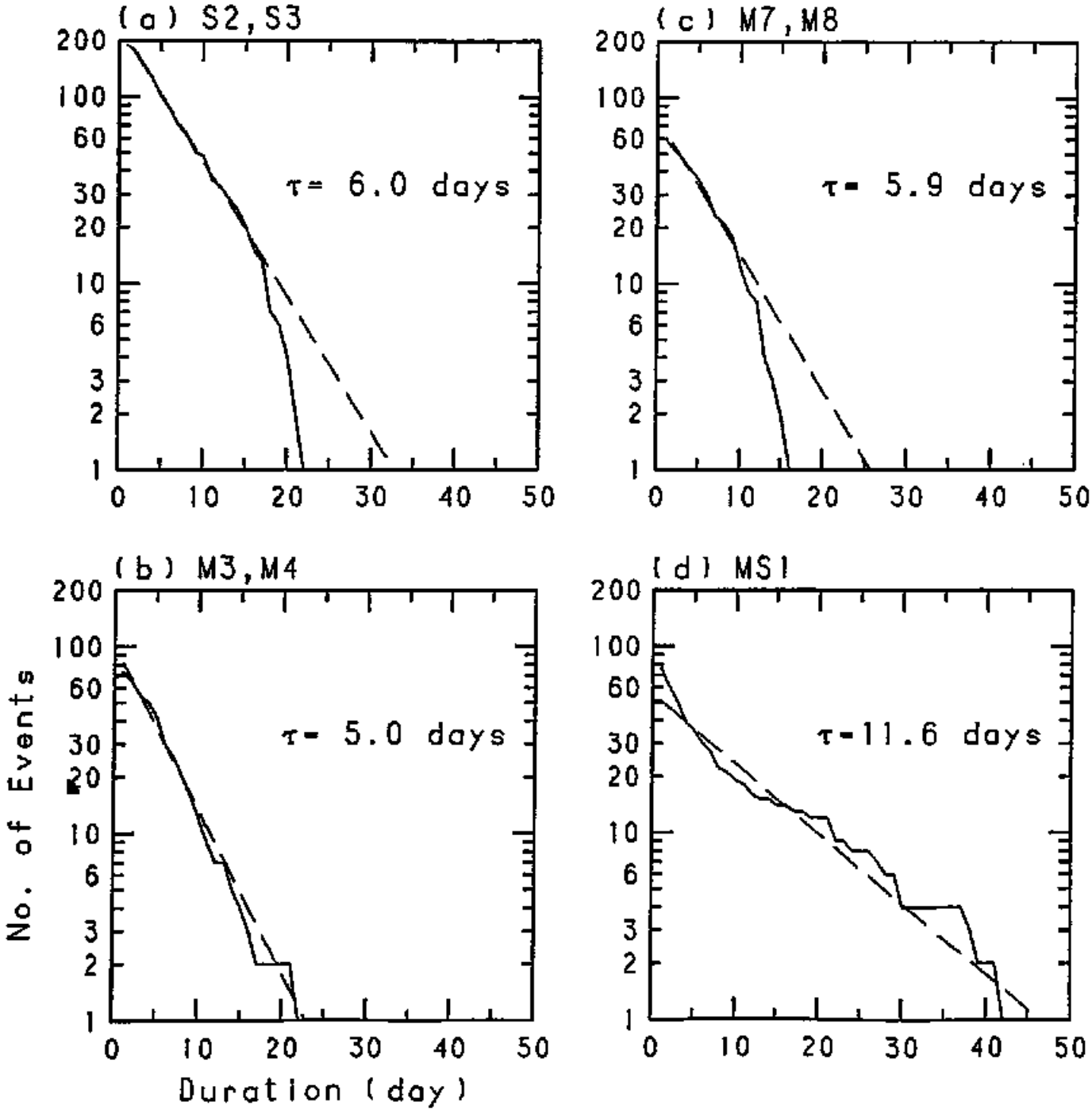

Fig.17. Persistence distribution of QS states in some groups occurring in the vicinity of the same MP at θ_A^*=0.054 (solid lines). All data sets in Table 2 are used. The ordinate is the total number of events which persist over n days on a *log*-scale and the abscissa is in days. Broken lines are computed using a least squares by $A \exp(-t/\tau)$. Each characteristic time τ is also presented.

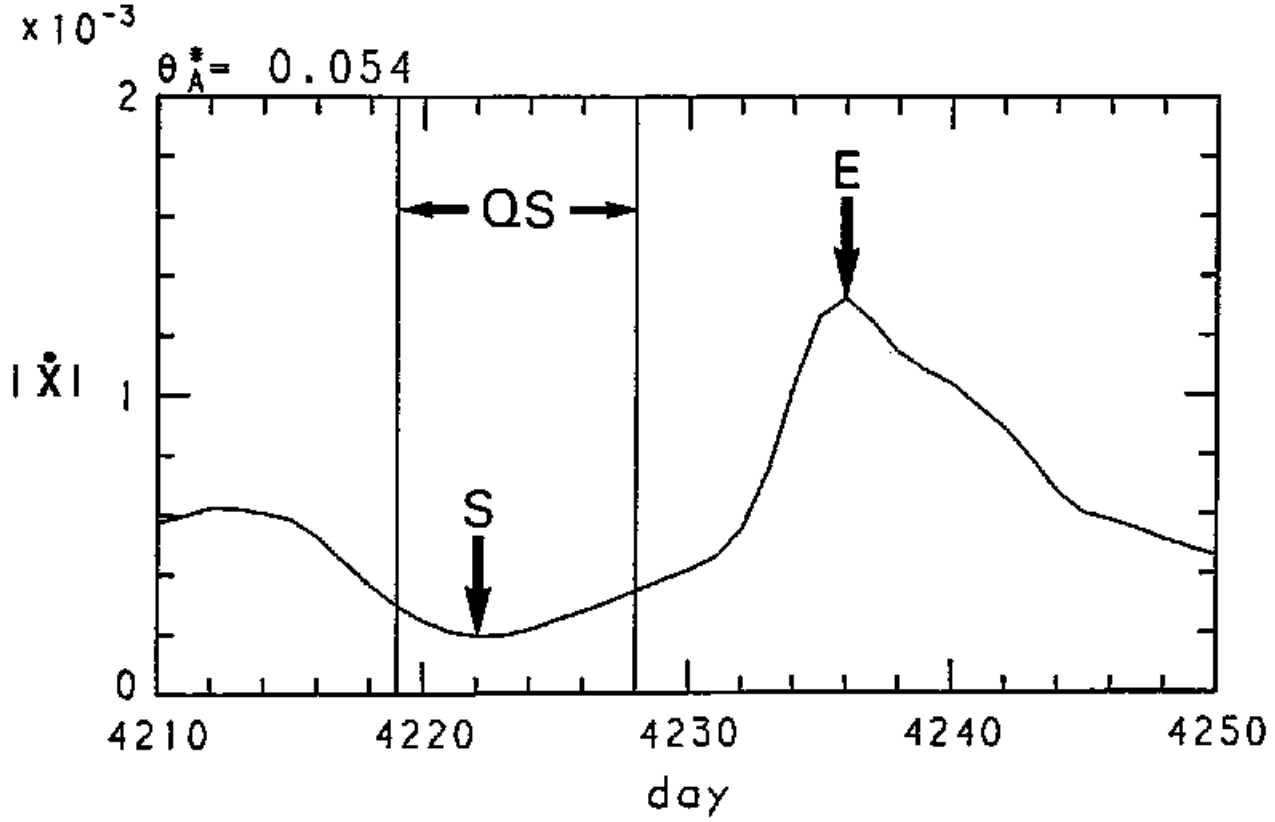

Fig.18. Same as in Fig.12. The period of a QS state is denoted by two vertical lines.

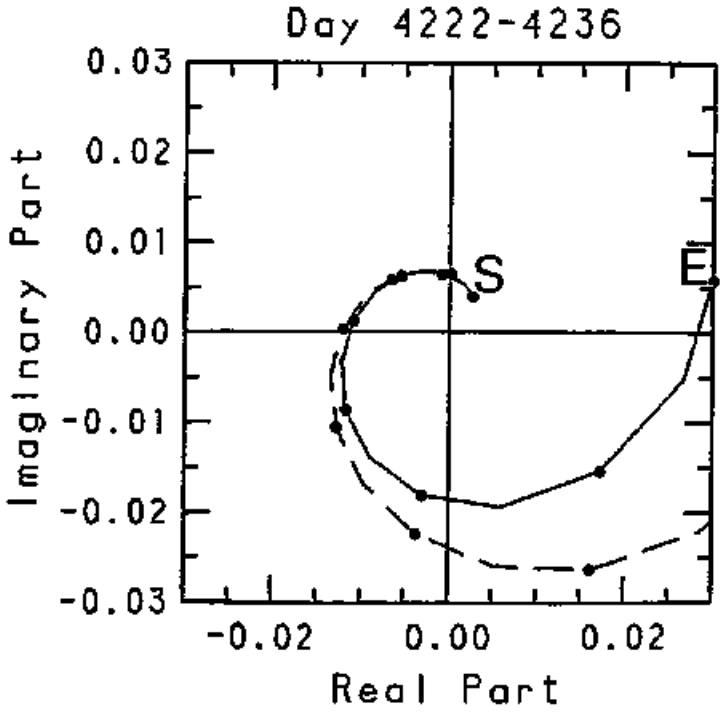

Fig.19. Time variation of complex expansion coefficient of the most unstable eigenmode of S2 for the deviation field from S2 from day 4222 (denoted by S) to day 4236 (denoted by E) (solid line). The abscissa is the real part and the ordinate the imaginary part. Broken line shows the assumed linear growth of this eigenmode from day 4222. Small dots are plotted every two days from day 4222.

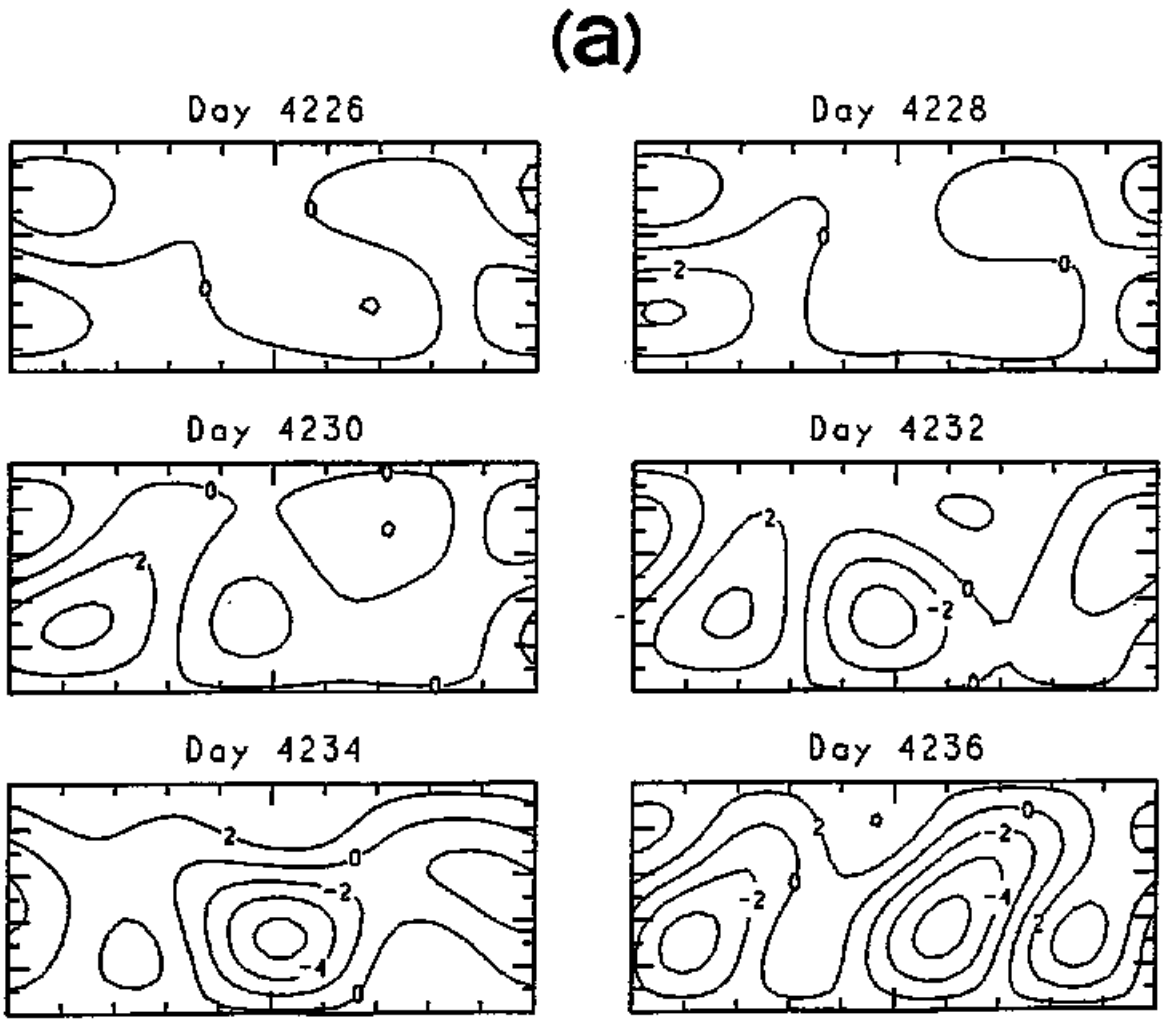

Fig.20. (a) Time variation of the upper-layer stream function of the deviation field from S2. (b) Time variation of the upper-layer stream function of the most unstable eigenmode of S2. Its amplitude is given by the expansion coefficient of this eigenmode for the deviation field.

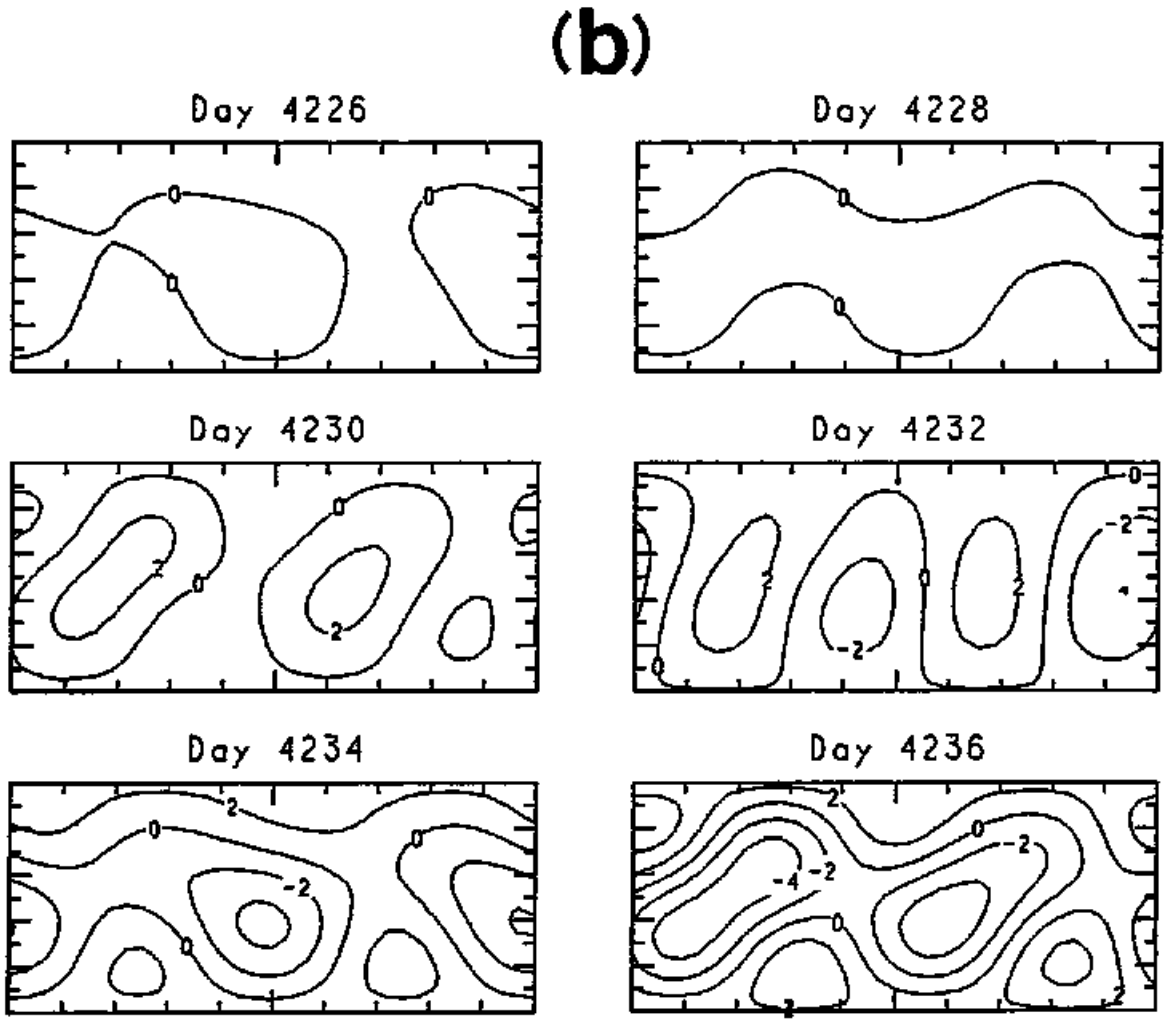

Fig. 20-(b)

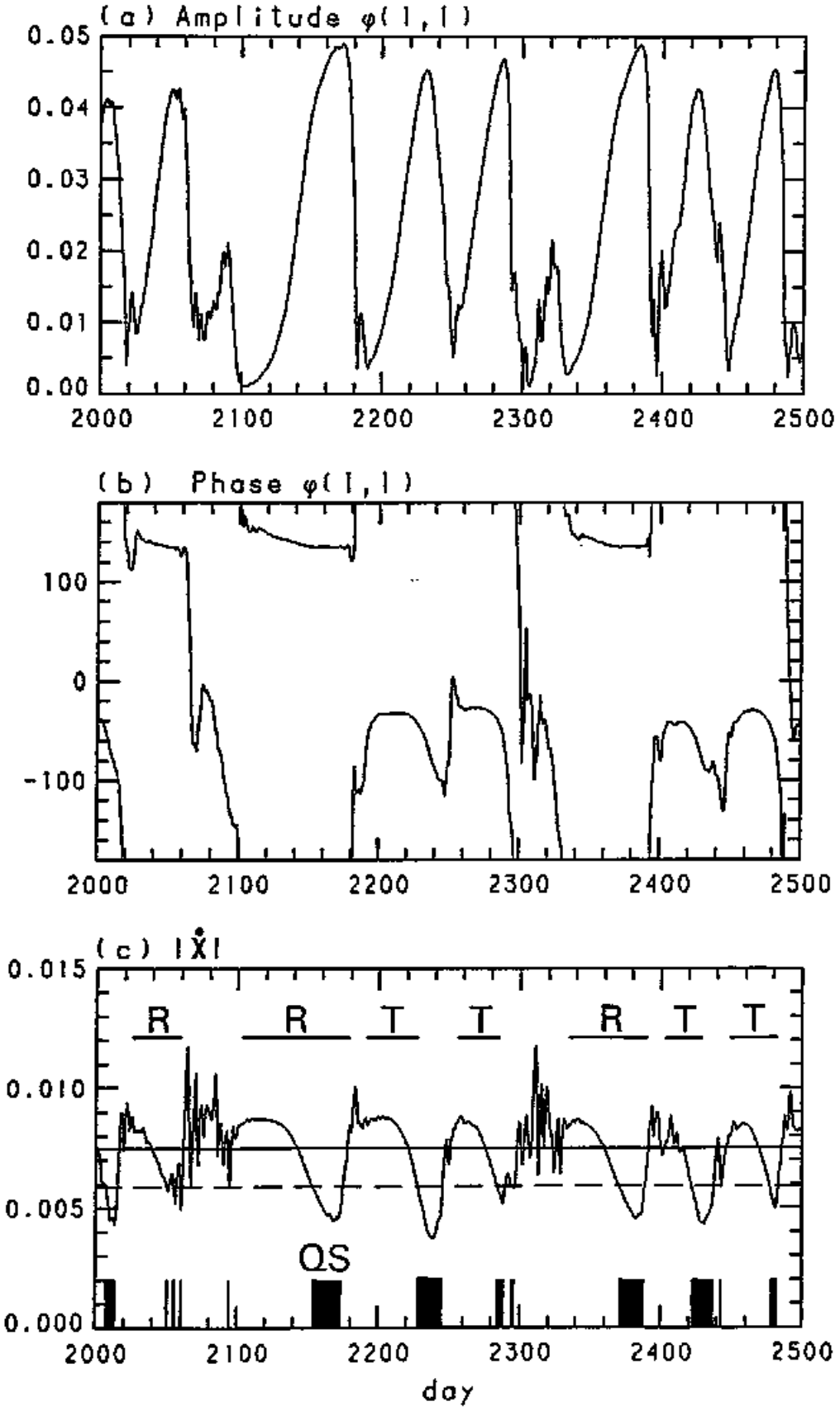

Fig.21 (a) Time variation of the amplitude of the gravest barotropic wave component in the demonstration case of RP. (b) As in (a) except for the phase. (c) As in (a) except for $|\dot{x}|$. Each period of the weather regime is denoted by R (ridge) and T (trough). Each QS state is indicated by a vertical line whose width is its period.

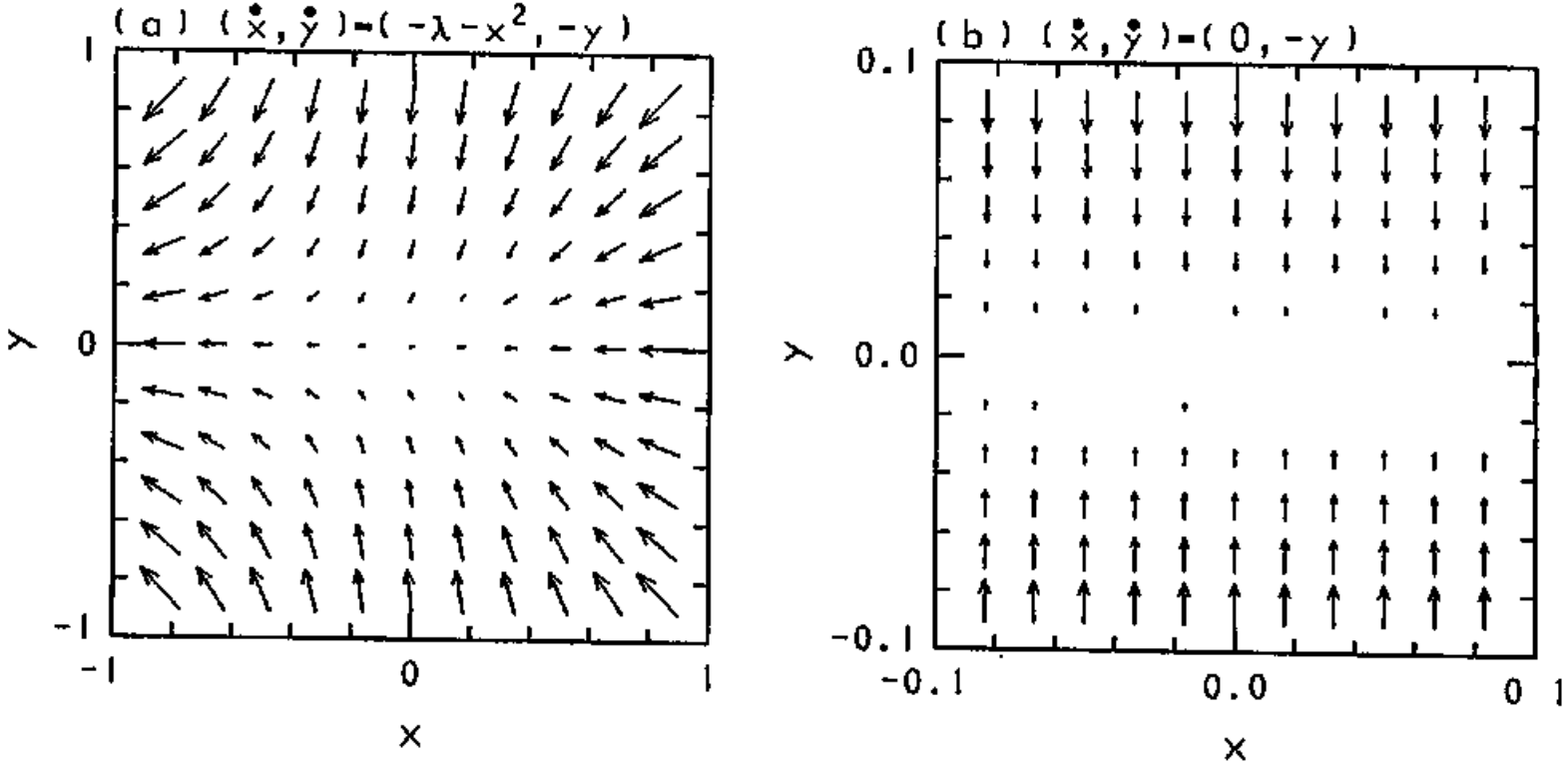

Fig.A1. (a) Flows in $(\dot{x}, \dot{y})=(-\lambda-x^2, -y)$ (λ=0.1). (b) The linearized flows of (a) around the MIN (the origin). Stable and zero eigenvector of the MIN is y-axis and x-axis, respectively.

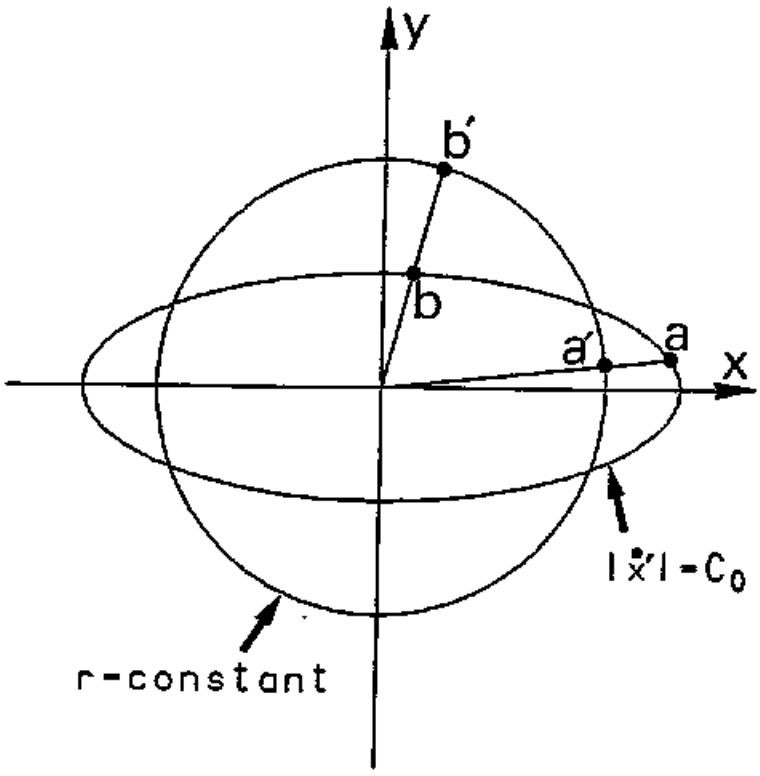

Fig.B1. The direction of the vector $\nabla|\dot{x}'_i|^2$ and $\dot{x}'_i$ at a point (*e.g.*, **a** and **b**) on the surface of $|\dot{x}'_i|=C_0$ is identical to that at the corresponding point (*e.g.*, **a'** and **b'**) on the ν-dimensional sphere (r=constant) for the linearized equation around an MP.

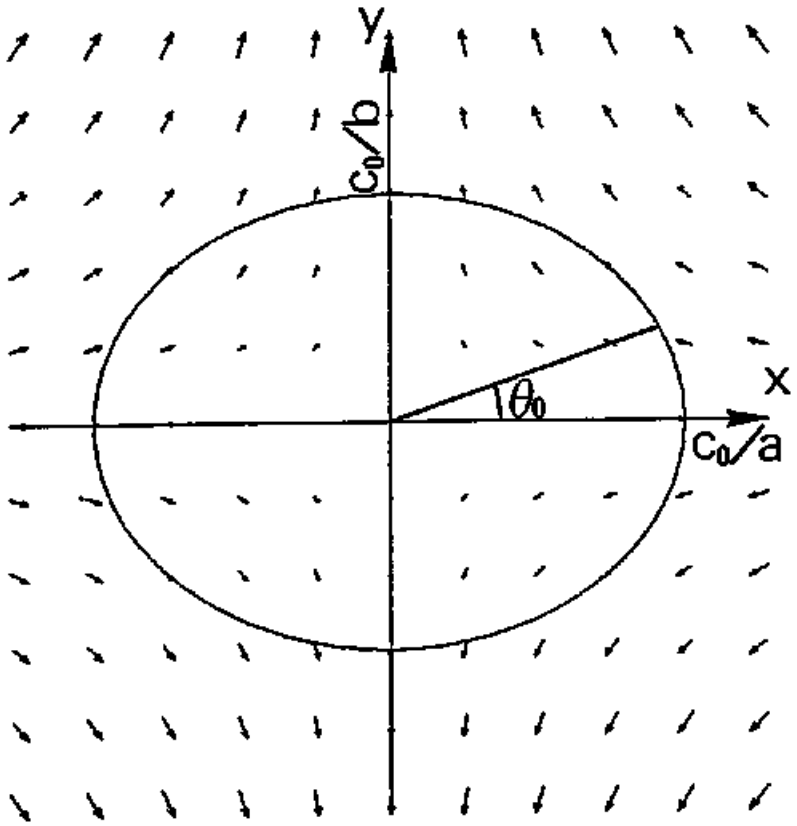

Fig.C1 Schematic diagram of flows in $(\dot{x}, \dot{y})=(-ax, by)$. The ellipsoid $a^2x^2+b^2y^2=C_0^2$ is drawn by solid line.

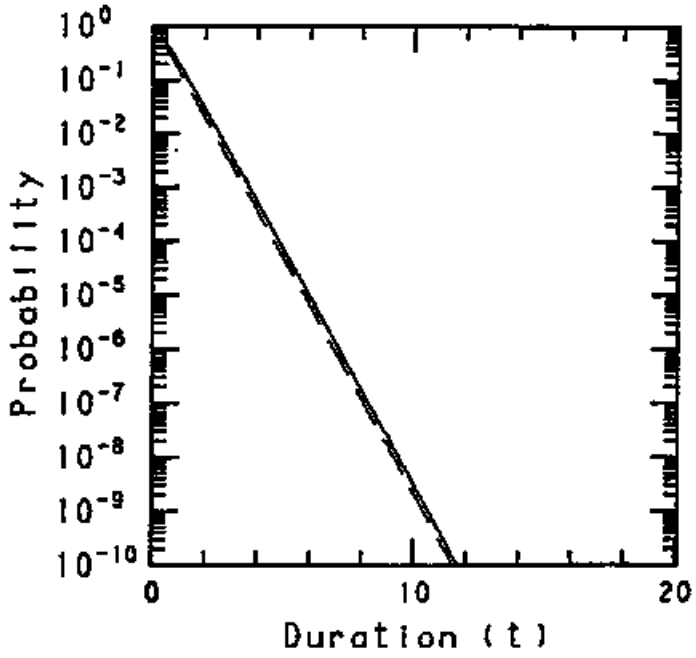

Fig.C2. Probability that a QS state persists over a time t in the system of $(\dot{x}, \dot{y})=(-ax, by)$ (solid line). Broken line shows the asymptotic behavior, e^{-bt} in the limit of $t\to\infty$.